

Constranits of dynamical dark energy models from different observational datasets

Peiyuan Xu¹, Lu Chen^{1*}, Guohao Li¹, Yang Han¹

¹ *School of Physics and Electronics, Shandong Normal University, Jinan 250014, China*

(Dated: October 14, 2025)

The measurements of baryon acoustic oscillation by the Dark Energy Spectroscopic Instrument Data Release 2 indicate that dark energy may be a dynamical quantity with a time-varying equation of state. This challenges the core assumptions of the Λ CDM model and has generated significant interest in dynamical dark energy models. Therefore, studying the parameterization of the equation of state for dynamical dark energy is crucial. Existing work has achieved fruitful results in the dark energy models, exploring various parameterization forms, but it is relatively scattered and lacks systematic parameter constraints based on the latest dataset combinations. We use the Λ CDM as a baseline model and carry out rigorous statistical constraints on key cosmological parameters for seven representative parameterization models. Planck PR4 and DESI DR2 observations are incorporated into our study. We use three dataset combinations: CMB+BAO+PantheonPlus, CMB+BAO+DES-Y5, and CMB+BAO+Union3. The H_0 and σ_8 values of all dynamical dark energy models are lower than the Λ CDM model, indicating that our results may not effectively alleviate H_0 tension, but can significantly reduce σ_8 tension. By comparing the χ^2 and the Akaike Information Criterion obtained for each model, we demonstrate that the linear Chevallier-Polarski-Linder parameterization model is not the optimal choice in all cases. Specifically, when combined with the CMB+BAO+DES-Y5 dataset, the Barboza-Alcaniz, Logarithmic, and Exponential models demonstrate superior statistical fitting performance compared to the Λ CDM model. The Barboza-Alcaniz model shows a great advantage in fitting performance, leading to the most significant improvement.

I. INTRODUCTION

In 1998, observations of distant Type Ia supernovae (SNIa) first suggested that our universe is undergoing accelerated expansion, which is one of the most important cosmological discoveries in the past three decades [1, 2]. The most successful theory to explain this phenomenon is dark energy. In the standard model of cosmology, the Λ -Cold Dark Matter (Λ CDM) model [3], the universe is composed of cold dark matter, baryons, negligible radiation and dark energy, where dark energy is considered to be the cosmological constant Λ , accounting for about 70% of the energy in the universe. Although the Λ CDM model has been in excellent agreement with a variety of observations for a long time, it also faces challenges from some well-known theoretical problems, such as Hubble tension, σ_8 tension et. al. [4–7].

Hubble tension refers to the significant difference between the value of Hubble constant H_0 , inferred from the Cosmic Microwave Background (CMB) and the value obtained through local distance ladder observations. In the Λ CDM framework, the value obtained using the Planck CMB+lensing is: 67.36 ± 0.54 km/s/Mpc [8]. However, local measurements conducted by the SH0ES team using the Cepheid variable calibrators show $H_0 = 73.04 \pm 1.04$ km/s/Mpc [6], a difference of 4.85σ . In comparison, the σ_8 tension is relatively low. The values of σ_8 obtained from Weak Lensing (WL), Cluster Counts (CC), or Redshift Space Distortion (RSD) are all significantly lower than the value of 0.811 ± 0.006 given by the Planck CMB TTTEEE+lowE+lensing [8], with a difference of 2-3 σ . These tensions pose increasing challenges to the standard cosmological model and may suggest the emergence of new physics beyond the Λ CDM model.

To better address these issues, the parameterized Dynamical Dark Energy (DDE) model emerged. Typically, the Dark Energy Equation of State (DE EOS) can be defined as $w = \frac{p_{de}}{\rho_{de}}$ to characterize the properties of dark energy, where p_{de} represents the pressure of dark energy and ρ_{de} represents its energy density. DDE model assumes that w is a constant different from -1 or evolves with time, thus constructing a flexible theoretical framework that allows for a more systematic exploration of potential deviations from the cosmological constant Λ . Various parameterized DDE models have been proposed. Among them, w CDM model is a minimal extension of the Λ CDM model, in which the DE EOS w is kept constant other than -1. The most representative and widely accepted two-parameter extension model is the CPL model. It can be expressed as: $w(a) = w_0 + w_a(1 - a)$.

From an observational perspective, *Planck* investigation of the anisotropy for CMB is of great significance to cosmology. However, the CMB data alone impose relatively limited constraints on DDE model. Even in simple two-parameter models designed to minimize degrees of freedom, the constraints generated by CMB are often too broad

* chenlu@sdsu.edu.cn

to provide rich and useful information. Therefore, observations of the local universe have assumed a more prominent position.

The Type Ia Supernovae DES-Y5, based on a joint compilation of PantheonPlus and Union3, found that, whether using SNIa alone or in combination with CMB and Baryon Acoustic Oscillations (BAO), the best fit EoS w is always slightly greater than -1 above the 1σ level. This is consistent with the constraints of Union3 and supports the trend of DDE. Dark Energy Spectroscopic Instrument (DESI) tracks the expansion of the universe using BAO observations [9–13]. When DESI DR1 is combined with Planck CMB and SNIa (Pantheonplus [14, 15], Union3 [16] and DESY5 [17–19]), the results show a clear tension with the Λ CDM model, giving a strong indication of DDE. Specifically, in the CPL model, $w_0 > -1$ and $w_a < 0$ have a clear preference at statistical levels between 2.5σ and 3.9σ [10]. This has sparked extensive discussion about dark energy. Inconsistencies between different datasets may be a reason for these discrepancies. For example, excluding the LRG1 ($z_{\text{eff}} = 0.51$) and LRG2 ($z_{\text{eff}} = 0.71$) individually results in $w = -1$ falling within the 2σ contour [20, 21]. In addition, the BAO measurement results of the Sloan Digital Sky Survey (SDSS) and DESI collaboration are also inconsistent with each other [22].

For DDE, the released DESI DR2 data further strengthen this preference [12, 23, 24]. The combination of DESI DR2 with CMB alone yields a significance of 3.1σ to the exclusion of Λ CDM. When combined with CMB, DESI DR2 and SNIa (PantheonPlus, Union3, and DES-Y5), this preference for DDE still exists, reaching significances of 2.8σ , 3.8σ and 4.2σ , respectively [12].

To comprehensively analyze various DDE parameterizations, we integrate cutting-edge observational data from current cosmological researches, focusing on the recently released CMB PR4 and DESI DR2 measurements. Based on these updated datasets and combined with three representative SNIa samples, we construct three core dataset combinations: CMB+BAO+PantheonPlus, CMB+BAO+DES-Y5, and CMB+BAO+Union3. Using the Λ CDM model as a benchmark framework, we conducted a comprehensive parameter constraint analysis on seven representative DDE parameterizations: w CDM, Chevallier-Polarski-Linder (CPL), Jassal-Bagla-Padmanabhan (JBP), Feng-Shen-Li-Li (FSL), Barboza-Alcaniz (BA), Logarithmic (LOG) and Exponential (EXP).

This paper is organized as follows. In Section II, we introduce the Friedmann equations and the evolution of dark energy. Section III describes the methods employed in our analysis and all observational datasets used. In Section IV, we give constraints on relevant parameters for all DDE parameterized models. Section V presents a comparative analysis of models and observational data, systematically discussing our results. Finally, a brief summary is included in Section VI.

II. DYNAMIC DARK ENERGY MODELS

The Friedmann equation describes the evolution of our universe. Considering a statistically homogeneous and isotropic universe that satisfies the Friedmann-Lemaître-Robertson-Walker (FLRW) metric, we can obtain:

$$H^2(a) = \frac{8\pi G}{3} [\rho_{r,0}a^{-4} + \rho_{m,0}a^{-3} + \rho_{de,0}X(a)]. \quad (1)$$

Here a represents the scale factor, $H(a)$ denotes the Hubble parameter and G is the Newton's gravitational constant. ρ is the energy density, subscript 0 indicates current values of the physical quantities, while subscripts r, m, and de are the radiation, matter, and dark energy, respectively. Meanwhile,

$$X(a) = \text{Exp} \left[-3 \int_{a_0=1}^a \frac{1+w(a)}{a} da \right]. \quad (2)$$

Where $w(a)$ represents the DE EOS as a function of the scale factor and it can be parameterized by w_0 and w_a . In the section IV, we will list the $X(a)$ of each DDE model separately to illustrate the evolution of dark energy density more intuitively.

III. METHODS

In this section, we summarize the statistical methods employed in our analysis and list the observational data combination used.

A. Statistical Analyses

We use the publicly available cosmological calculation code CAMB [25, 26], and make specific modifications for different models. Then we perform Markov Chain Monte Carlo (MCMC) analysis with the publicly available sampler Cobaya [27, 28]. The convergence of the generated MCMC chains is evaluated by the Gelman-Rubin parameter $R - 1$ [29]. For all models and datasets, we require that the chains are considered convergent only when the condition $R - 1 < 0.01$ is satisfied. All DDE models listed in Section IV can be characterized by 8 free parameters: $\{\Omega_c h^2, \Omega_b h^2, A_s, n_s, \tau, \theta_{\text{MC}}, w_0, w_a\}$. $\Omega_c h^2$ is the physical cold dark matter energy density; $\Omega_b h^2$ is the physical baryon energy density; A_s is the primordial scalar spectrum amplitude; n_s is the spectrum index; τ is the reionization optical depth; θ_{MC} is the angular size of the sound horizon. The DE EOS has two free parameters: w_0 , which is its current value, and w_a , which describes its time variation. In TABLE I, we give the flat prior ranges of the free variation of the parameters.

Parameter	Prior
$\Omega_b h^2$	[0.005, 0.1]
$\Omega_c h^2$	[0.001, 0.99]
$\log(10^{10} A_s)$	[1.61, 3.91]
n_s	[0.8, 1.2]
τ	[0.01, 0.8]
$100\theta_{\text{MC}}$	[0.5, 10]
w_0	[-3, 1]
w_a	[-3, 2]

TABLE I: The range of flat prior distributions of free cosmological parameters in our analysis.

B. Datasets

Here we list all data and corresponding references used in our analysis.

- **CMB:** We use the combination of Planck TTEE+lowE data from the Planck 2018 observation [8], the latest NPIPE (PR4) CamSpec high- l TTTEEE likelihood [30, 31], and the Planck PR4 lensing [32].
- **BAO:** We adopt the BAO measurements from DESI DR2 in the range $0.1 < z < 4.2$ [12, 33].
- **PantheonPlus SNe:** We utilize the PantheonPlus sample [14, 15] consisting of 1550 SNIa over the redshift range $0.001 < z < 2.26$.
- **DES-Y5 SNe:** We employ the DES-Y5 sample [17–19], which includes 1635 light curves from 1550 SNIa in the redshift range $0.10 < z < 1.13$, along with 194 low-redshift SNIa in the range $0.025 < z < 0.10$.
- **Union3 SNe:** We use an updated “Union” compilation consisting of 2087 cosmologically useful SNIa from 24 datasets (“Union3”) [16].

We tested these models using three different datasets: CMB+BAO+PantheonPlus, CMB+BAO+DES-Y5 and CMB+BAO+Union3.

IV. RESULTS

In this section, we detail the constraints on the Λ CDM and seven DDE models included in our study. Subsequently, we analyze the parameter results of each model in turn. The results of all tests are presented in Table II. This table combines horizontal and vertical presentation: horizontally, the parameter results for the same model under different datasets are compared, while vertically, the parameter results for all models under the same dataset are presented.

The parameters discussed in this article mainly include three free parameters: w_0 , w_a and $\Omega_c h^2$; three derived parameters: Ω_m , σ_8 and H_0 . We only list the above because the changes of other parameters compared with the Planck CMB are very small and can be ignored. Figures 1 - 9 show the full triangle plots of the Λ CDM, w CDM, CPL, JBP, FSL I, FSL II, BA, LOG, and EXP models under the constraints of three datasets: CMB+BAO+PantheonPlus,

CMB+BAO+DES-Y5, and CMB+BAO+Union3, respectively. Figures 10 - 12 show the complete triangle diagrams of all two-parameter DDE models under the constraints of the three datasets described above.

TABLE II: The 68% limits of the cosmological parameters for all models under the combination of CMB+BAO+ PantheonPlus, CMB+BAO+DES-Y5, and CMB+BAO+Union3 datasets.

Model	CMB+BAO+PantheonPlus	CMB+BAO+DES-Y5	CMB+BAO+Union3
ΛCDM			
$\Omega_c h^2$	0.11780 ± 0.00059	0.11798 ± 0.00060	0.11777 ± 0.00061
Ω_m	$0.3035^{+0.0034}_{-0.0035}$	0.3046 ± 0.0035	0.3033 ± 0.0035
σ_8	$0.8060^{+0.0057}_{-0.0056}$	$0.8061^{+0.0056}_{-0.0055}$	0.8060 ± 0.0056
H_0 [km/s/Mpc]	68.10 ± 0.27	68.02 ± 0.27	68.12 ± 0.28
χ^2	12406.8	12650.2	11029.4
AIC	12418.8	12662.2	11041.4
wCDM			
$\Omega_c h^2$	$0.11764^{+0.00074}_{-0.00075}$	0.11737 ± 0.00074	$0.11765^{+0.00074}_{-0.00076}$
w_0	$-0.992^{+0.025}_{-0.023}$	-0.969 ± 0.021	-0.994 ± 0.027
Ω_m	$0.3048^{+0.0050}_{-0.0051}$	$0.3098^{+0.0048}_{-0.0049}$	$0.3044^{+0.0060}_{-0.0058}$
σ_8	0.8038 ± 0.0086	$0.7972^{+0.0085}_{-0.0084}$	$0.8042^{+0.0094}_{-0.0092}$
H_0 [km/s/Mpc]	$67.93^{+0.57}_{-0.56}$	67.32 ± 0.53	67.98 ± 0.68
χ^2	12407.7	12648.9	11030.5
AIC	12421.7	12662.9	11044.5
CPL			
$\Omega_c h^2$	$0.11719^{+0.00067}_{-0.00068}$	0.11707 ± 0.00071	0.11717 ± 0.00068
w_0	$-0.967^{+0.010}_{-0.030}$	$-0.942^{+0.024}_{-0.033}$	$-0.959^{+0.013}_{-0.040}$
w_a	$-0.005^{+0.030}_{-0.037}$	$-0.032^{+0.035}_{-0.045}$	$-0.016^{+0.039}_{-0.041}$
Ω_m	$0.3087^{+0.0042}_{-0.0050}$	$0.3130^{+0.0046}_{-0.0056}$	$0.3106^{+0.0047}_{-0.0062}$
σ_8	$0.7969^{+0.0076}_{-0.0069}$	$0.7920^{+0.0087}_{-0.0077}$	$0.7950^{+0.0090}_{-0.0074}$
H_0 [km/s/Mpc]	$67.40^{+0.52}_{-0.39}$	$66.91^{+0.59}_{-0.48}$	$67.19^{+0.68}_{-0.46}$
χ^2	12408.3	12648.5	11030.9
AIC	12424.3	12664.5	11046.9
JBP			
$\Omega_c h^2$	$0.11720^{+0.00069}_{-0.00063}$	$0.11713^{+0.00070}_{-0.00071}$	$0.11720^{+0.00070}_{-0.00069}$
w_0	$-0.979^{+0.006}_{-0.021}$	$-0.964^{+0.015}_{-0.029}$	$-0.974^{+0.008}_{-0.025}$
w_a	$0.044^{+0.031}_{-0.072}$	$0.034^{+0.038}_{-0.084}$	$0.039^{+0.034}_{-0.073}$
Ω_m	0.3079 ± 0.0043	$0.3112^{+0.0045}_{-0.0049}$	$0.3089^{+0.0043}_{-0.0051}$
σ_8	$0.7975^{+0.0074}_{-0.0068}$	$0.7938^{+0.0078}_{-0.0076}$	$0.7965^{+0.0080}_{-0.0070}$
H_0 [km/s/Mpc]	$67.49^{+0.45}_{-0.40}$	$67.11^{+0.51}_{-0.45}$	$67.38^{+0.54}_{-0.41}$
χ^2	12408.6	12649.4	11031.3
AIC	12424.6	12665.4	11047.3
FSLL I			
$\Omega_c h^2$	$0.11721^{+0.00069}_{-0.00067}$	0.11708 ± 0.00070	$0.11718^{+0.00068}_{-0.00069}$
w_0	$-0.971^{+0.009}_{-0.028}$	$-0.948^{+0.024}_{-0.032}$	$-0.964^{+0.011}_{-0.035}$
w_a	$0.004^{+0.030}_{-0.043}$	$-0.020^{+0.035}_{-0.051}$	$-0.003^{+0.036}_{-0.045}$
Ω_m	$0.3085^{+0.0042}_{-0.0048}$	$0.3123^{+0.0046}_{-0.0051}$	$0.3097^{+0.0046}_{-0.0056}$
σ_8	$0.7972^{+0.0078}_{-0.0072}$	0.7927 ± 0.0080	$0.7958^{+0.0084}_{-0.0070}$
H_0 [km/s/Mpc]	$67.42^{+0.49}_{-0.40}$	$66.98^{+0.52}_{-0.51}$	$67.28^{+0.60}_{-0.46}$
χ^2	12408.3	12648.6	11031
AIC	12424.3	12664.6	11047
FSLL II			
$\Omega_c h^2$	0.11721 ± 0.00068	$0.11710^{+0.00070}_{-0.00069}$	0.11717 ± 0.00068
w_0	$-0.968^{+0.011}_{-0.029}$	$-0.945^{+0.024}_{-0.027}$	$-0.959^{+0.014}_{-0.037}$
w_a	$-0.006^{+0.027}_{-0.036}$	$-0.030^{+0.030}_{-0.040}$	$-0.015^{+0.033}_{-0.039}$
Ω_m	$0.3087^{+0.0043}_{-0.0050}$	0.3131 ± 0.0051	$0.3104^{+0.0049}_{-0.0061}$
σ_8	$0.7971^{+0.0073}_{-0.0074}$	$0.7922^{+0.0080}_{-0.0079}$	$0.7952^{+0.0086}_{-0.0077}$
H_0 [km/s/Mpc]	$67.41^{+0.53}_{-0.41}$	66.90 ± 0.53	$67.20^{+0.67}_{-0.48}$
χ^2	12408	12647.9	11030.7
AIC	12424	12663.9	11046.7

TABLE II

Model	CMB+BAO+PantheonPlus	CMB+BAO+DES-Y5	CMB+BAO+Union3
BA			
$\Omega_c h^2$	$0.11723^{+0.00066}_{-0.00065}$	0.11718 ± 0.00066	$0.11715^{+0.00066}_{-0.00067}$
w_0	$-0.938^{+0.028}_{-0.040}$	-0.892 ± 0.037	$-0.882^{+0.051}_{-0.058}$
w_a	$-0.047^{+0.041}_{-0.035}$	-0.095 ± 0.041	$-0.104^{+0.058}_{-0.057}$
Ω_m	$0.3111^{+0.0050}_{-0.0055}$	$0.3174^{+0.0055}_{-0.0054}$	$0.3187^{+0.0071}_{-0.0082}$
σ_8	0.7951 ± 0.0074	0.7892 ± 0.0074	0.7877 ± 0.0093
H_0 [km/s/Mpc]	$67.15^{+0.56}_{-0.50}$	$66.47^{+0.55}_{-0.54}$	$66.33^{+0.81}_{-0.78}$
χ^2	12406.2	12643.2	11027.2
AIC	12422.2	12659.2	11043.2
LOG			
$\Omega_c h^2$	$0.11722^{+0.00067}_{-0.00066}$	$0.11708^{+0.00068}_{-0.00067}$	$0.11713^{+0.00068}_{-0.00069}$
w_0	$-0.955^{+0.019}_{-0.034}$	-0.920 ± 0.031	$-0.931^{+0.030}_{-0.048}$
w_a	$-0.028^{+0.034}_{-0.031}$	$-0.063^{+0.033}_{-0.039}$	$-0.052^{+0.049}_{-0.039}$
Ω_m	$0.3098^{+0.0045}_{-0.0054}$	0.3152 ± 0.0052	$0.3136^{+0.0058}_{-0.0072}$
σ_8	$0.7962^{+0.0075}_{-0.0076}$	0.7903 ± 0.0078	$0.7923^{+0.0093}_{-0.0083}$
H_0 [km/s/Mpc]	$67.28^{+0.56}_{-0.44}$	$66.67^{+0.54}_{-0.53}$	$66.86^{+0.77}_{-0.61}$
χ^2	12407.2	12645.7	11029.7
AIC	12423.2	12661.7	11045.7
EXP			
$\Omega_c h^2$	$0.11726^{+0.00066}_{-0.00065}$	$0.11712^{+0.00065}_{-0.00066}$	$0.11713^{+0.00068}_{-0.00069}$
w_0	$-0.971^{+0.012}_{-0.016}$	$-0.956^{+0.013}_{-0.014}$	$-0.958^{+0.017}_{-0.019}$
w_a	$-0.011^{+0.014}_{-0.016}$	$-0.029^{+0.013}_{-0.015}$	$-0.026^{+0.020}_{-0.019}$
Ω_m	$0.3102^{+0.0052}_{-0.0058}$	0.3166 ± 0.0055	$0.3155^{+0.0070}_{-0.0080}$
σ_8	$0.7964^{+0.0078}_{-0.0079}$	$0.7901^{+0.0075}_{-0.0076}$	0.7911 ± 0.0090
H_0 [km/s/Mpc]	$67.25^{+0.58}_{-0.57}$	66.54 ± 0.56	$66.66^{+0.80}_{-0.78}$
χ^2	12407.3	12644.4	11028.9
AIC	12423.3	12660.4	11044.9

1. Λ CDM

The Λ CDM is included as the standard model in our work, where $w_0 = -1$, $w_a = 0$, to compare with other models. The parameter constraints obtained by Λ CDM in three different datasets do not change much, showing high stability.

We compare our H_0 results with $H_0 = 67.36 \pm 0.54$ km/s/Mpc given by Planck PR3 TTTEEE+lowE+lensing (hereafter Planck PR3) [8] and the local measurement result of $H_0 = 73.04 \pm 1.04$ km/s/Mpc (hereafter Local) [6]. Under CMB+BAO+PantheonPlus, $H_0 = 68.10 \pm 0.27$ km/s/Mpc, 1.23σ difference compared to Planck PR3 and 4.60σ difference compared to Local. Under CMB+BAO+DES-Y5, $H_0 = 68.02 \pm 0.27$ km/s/Mpc, 1.09σ difference compared to Planck PR3 and 4.67σ difference compared to Local. Finally, under CMB+BAO+Union3, $H_0 = 68.12 \pm 0.28$ km/s/Mpc, resulting in a 1.25σ difference compared to Planck PR3 and a 4.57σ difference compared to Local.

As can be seen in Figure 1, H_0 is inversely proportional to both $\Omega_c h^2$ and Ω_m , while Ω_m is positively correlated with $\Omega_c h^2$. This indicates that the change in Ω_m may come mainly from Ω_c .

The values of σ_8 in Λ CDM are also completely consistent across the three datasets. Changing only the SNIa has little impact on the σ_8 constraint. Taking CMB+BAO+Union3 as an example, $\sigma_8 = 0.8060 \pm 0.0056$. Compared to the value $\sigma_8 = 0.811 \pm 0.006$ under the Planck PR3 TTTEEE+lowE+lensing [8], the difference is minimal, just 0.61σ . Compared to the σ_8 value of 0.819 ± 0.015 obtained from the combination of ACT DR6 and BAO (6df and SDSS) [34], there is a 0.81σ discrepancy. Compared with $\sigma_8 = 0.783^{+0.073}_{-0.092}$ from DES-Y3 [35, 36], the difference is 0.31σ . Although the difference between our result and DES-Y3 is reduced, it is mainly because the error bar of the data provided by DES-Y3 is too large, which leads to broad constraints. Our results in Λ CDM do not provide new implications for the σ_8 tension.

2. w CDM

In w CDM model, w_0 is a variable constant and $w_a = 0$. This model, as the smallest extension of the Λ CDM, is the only single-parameter DDE model included in our study. w_0 describes the evolution of DE EOS and shows the lowest

value under the constraints of three different datasets. Specifically, $w_0 = -0.992^{+0.025}_{-0.023}$ in CMB+BAO+PantheonPlus; $w_0 = -0.969 \pm 0.021$ in CMB+BAO+DES-Y5; and $w_0 = -0.994 \pm 0.027$ in CMB+BAO+Union3.

Our constraints on w_0 show high consistency with the results from [12], which also uses the DESI DR2 and three SNIa datasets, with only slight differences in the CMB data: a combination of Planck TTTEEE SimAll, Commander ($l < 30$) and CamSpec ($l \geq 30$) likelihoods, including Planck and ACT DR6 lensing. In DESI+CMB+PantheonPlus, $w_0 = -0.995 \pm 0.023$; in DESI+CMB+DES-Y5, $w_0 = -0.971 \pm 0.021$; and in DESI+CMB+Union3, $w_0 = -0.997 \pm 0.027$. The constraints indicate that variations for the CMB data have not significantly affected w_0 in w CDM model. Compared to the result $w_0 = -1.028 \pm 0.031$ from [8], the difference is 0.93σ for CMB+BAO+PantheonPlus; 1.58σ for CMB+BAO+DES-Y5; and 0.83σ for CMB+BAO+Union3. The data combination used is Planck TT+TEEE+lowE+lensing+SNIa (Pantheon)+BAO, where BAO utilizes the 6dFGS and SDSS-MGS measurements of D_V/r_{drag} [37, 38], as well as the final anisotropic BAO measurements of DR12 [39].

The H_0 value of the w CDM model is higher than all two-parameter DDE models, but lower than the Λ CDM model. Compared with 67.36 ± 0.54 from Planck PR3 [8] and $H_0 = 73.04 \pm 1.04$ km/s/Mpc from Local [6], $H_0 = 67.93^{+0.57}_{-0.56}$ km/s/Mpc in CMB+BAO+PantheonPlus differs by 0.73σ for PR3, 4.31σ for Local; $H_0 = 67.32 \pm 0.53$ km/s/Mpc under CMB+BAO+DES-Y5 differs by 0.05σ for PR3, 4.90σ for Local; and $H_0 = 67.98 \pm 0.68$ km/s/Mpc for CMB+BAO+Union3, with a difference of 0.71σ for PR3, 4.07σ for Local. Compared to Λ CDM, the error bars of H_0 for w CDM are slightly larger. It is precisely this wider constraint that allows the w CDM model to alleviate the H_0 tension, which is most significant when combined with the CMB+BAO+Union3 dataset.

Our constraints for Ω_m are $0.3048^{+0.0050}_{-0.0051}$ in CMB+BAO+PantheonPlus, $0.3098^{+0.0048}_{-0.0049}$ in CMB+BAO+DES-Y5, $0.3044^{+0.0060}_{-0.0058}$ in CMB+BAO+Union3. Compared with $\Omega_m = 0.3153 \pm 0.0073$ from Planck PR3 [8], the differences for three datasets are 1.19σ , 0.63σ and 1.15σ , respectively. [40] uses the DESI DR1+DES-Y5+Cosmic Chronometers+Strong Gravitational Lensing dataset. Its constraint value is $\Omega_m = 0.295 \pm 0.014$, which has a difference of 1.00σ with $0.3098^{+0.0048}_{-0.0049}$ in CMB+BAO+DES-Y5. Our result has a smaller error bar, reduced by about an order of magnitude.

3. CPL

Chevallier-Polarski-Linder (CPL) parametrization [41, 42] is the most basic and widely applicable two-parameter extension model, and its DE EOS is:

$$w(a) = w_0 + w_a(1 - a). \quad (3)$$

$X(a)$ under CPL parameterization is:

$$X(a) = a^{-3-3w_0-3w_a} \text{Exp}[3w_a(a-1)]. \quad (4)$$

The values of our w_0 show a consistent pattern: the 1σ confidence interval excludes the current value of DE EOS -1. In particular, w_0 under the CMB+BAO+DES-Y5 still deviates from -1 at the 2σ level, reaching $w_0 = -0.942^{+0.055}_{-0.054}$ at 95% C.L., which is a significant difference from the Λ CDM model. Furthermore, as clearly observed in Figure 3, under the constraints of the CMB+BAO+PantheonPlus and CMB+BAO+Union3, the one-dimensional distribution plots of w_0 present non-smooth distribution curves. However, replacing the SNIa data with DES-Y5 changes the situation, with the one-dimensional distribution of w_0 returning to a smooth single-peaked state.

Compared with $w_0 = -0.957 \pm 0.080$, $w_a = -0.29^{+0.32}_{-0.26}$ provided by Planck PR3+BAO+Pantheon [8], our results in CMB+BAO+PantheonPlus are $w_0 = -0.967^{+0.010}_{-0.030}$, $w_a = -0.005^{+0.030}_{-0.037}$, the divergence is 0.12σ for w_0 , 0.88σ for w_a ; in CMB+BAO+DES-Y5 are $w_0 = -0.942^{+0.024}_{-0.033}$, $w_a = -0.032^{+0.035}_{-0.045}$, the divergence is 0.17σ for w_0 , 0.80σ for w_a ; and in CMB+BAO+Union3 are $w_0 = -0.959^{+0.013}_{-0.040}$, $w_a = -0.016^{+0.039}_{-0.041}$, which has 0.02σ for w_0 and 0.85σ for w_a . In comparison, the difference in w_0 is negligible and in w_a is also controlled within 1σ , which means that this result is generally good in consistency. When we use our constraint of CMB+BAO+PantheonPlus to compare $w_0 = -0.829 \pm 0.088$ and $w_a = -0.09 \pm 0.11$ from [43], w_0 has a 1.54σ discrepancy, with the error bar reduced by 77%; w_a has a 0.73σ discrepancy, with the error bar reduced by 69%. [43] comprehensively utilizes various datasets. For CMB, it uses Planck 2018 TTTEEE+low l +lowE+lensing; for BAO, it combines 6dFGS, SDSS MGS, BOSS DR12 (LOWZ, CMASS and LRG), and eBOSS DR16 (galaxies, LRG, QSO, ELG, Ly α and Ly $\alpha \times$ QSO); meanwhile, SNIa (PantheonPlus) is also incorporated.

The Hubble constant $H_0 = 67.36 \pm 0.54$ km/s/Mpc from Planck PR3 [8] and $H_0 = 73.04 \pm 1.04$ km/s/Mpc from Local [6]. In CMB+BAO+PantheonPlus, $H_0 = 67.40^{+0.52}_{-0.39}$ km/s/Mpc, 0.06σ difference for Planck PR3 and 4.85σ difference for Local. In CMB+BAO+DES-Y5, $H_0 = 66.91^{+0.59}_{-0.48}$ km/s/Mpc, 0.56σ difference for Planck PR3 and 5.13σ difference for Local. In CMB+BAO+Union3, $H_0 = 67.19^{+0.68}_{-0.46}$ km/s/Mpc, 0.20σ divergence for Planck PR3 and 4.71σ divergence compared to Local.

Comparing with $\Omega_m = 0.3153 \pm 0.0073$ from Planck PR3 TTTEEE+lowE+lensing [8], we get a difference of 0.78σ for CMB+BAO+PantheonPlus; a 0.27σ difference for CMB+BAO+DES-Y5; and a 0.54σ difference for CMB+BAO+Union3. On the other hand, our result under CMB+BAO+DES-Y5 ($\Omega_m = 0.3130^{+0.0046}_{-0.0056}$) has 1.02σ different from $\Omega_m = 0.329^{+0.018}_{-0.015}$ [40]. [12] provides tight constraints on Ω_m . In DESI+CMB+PantheonPlus, $\Omega_m = 0.3114 \pm 0.0057$, a difference of 0.38σ ; in DESI+CMB+DES-Y5, $\Omega_m = 0.3191 \pm 0.0056$, a difference of 0.83σ ; and in DESI+CMB+Union3, $\Omega_m = 0.3275 \pm 0.0086$, a difference of 1.72σ . Since H_0 and Ω_m show a clear inverse relationship, in order to increase the H_0 as much as possible to ease the H_0 tension, our Ω_m results are relatively small, but the differences are all controlled within 2σ , and overall agreement is good.

4. Jassal-Bagla-Padmanabhan parametrization

We consider the Jassal-Bagla-Padmanabhan (JBP) [44] form for the DE EOS:

$$w(a) = w_0 + w_a a(1 - a). \quad (5)$$

Its $X(a)$ is :

$$X(a) = a^{-3-3w_0} \text{Exp} \left[\frac{3}{2} w_a (a-1)^2 \right]. \quad (6)$$

In CMB+BAO+PantheonPlus and CMB+BAO+Union3 datasets, the results for w_0 at the 1σ level. are very close to the standard value -1, with values of $-0.979^{+0.006}_{-0.021}$ and $-0.974^{+0.008}_{-0.025}$ at 68% C.L., respectively. In contrast, the constraint of w_0 in CMB+BAO+DES-Y5 slightly deviates from -1 at the 2σ level, with a value of $-0.964^{+0.041}_{-0.035}$ at 95% C.L..

From Figure 4, we find that the constraints of CMB+BAO+PantheonPlus and CMB+BAO+Union3 are similar, while the parameters under the constraint of CMB+BAO+DES-Y5 are slightly different. The probability of $w_0 > -1$ is higher under the former two datasets than under the latter. However, the constraints on w_a of the three datasets are very similar. Ω_m has an obvious inverse correlation with both H_0 and σ_8 parameters, while H_0 and σ_8 have a positive correlation.

We obtain $w_0 = -0.974^{+0.008}_{-0.025}$ and $w_a = 0.039^{+0.034}_{-0.073}$ in CMB+BAO+Union3. [45] also exhibits constraints of the DE EOS parameters when combined with Planck 2018+DESI DR2+Union3. Specifically, compared to our result, $w_0 = -0.621^{+0.130}_{-0.093}$, the difference is 3.78σ ; $w_a = -1.860^{+0.490}_{-0.730}$, which is 3.83σ lower than our result. Our constraining capabilities have improved significantly, for w_0 , the error bar decreases by 85%; for w_a , the error bar decreases by 91%. The CMB data that we used are different, which leads to significant discrepancies.

Compared to the Λ CDM model, the JBP model yields lower H_0 values when constrained by all three datasets, which undoubtedly exacerbates H_0 tension. Specifically, compared to $H_0 = 67.36 \pm 0.54$ km/s/Mpc from Planck PR3 [8] and the locally measured Hubble constant $H_0 = 73.04 \pm 1.04$ km/s/Mpc [6]. In CMB+BAO+PantheonPlus, $H_0 = 67.49^{+0.45}_{-0.40}$ km/s/Mpc, which has a difference of 0.19σ for Planck PR3, 4.90σ for Local; $H_0 = 67.11^{+0.51}_{-0.45}$ km/s/Mpc from CMB+BAO+DES-Y5, 0.34σ for Planck PR3 and 5.12σ for Local; and based on CMB+BAO+Union3, $H_0 = 67.38^{+0.54}_{-0.41}$ km/s/Mpc, with 0.03σ for Planck PR3, 4.83σ for Local.

Our results, based on the latest DESI DR2 and CMB PR4, provide tighter σ_8 constraints and alleviated σ_8 tension. Specifically, we obtain $\sigma_8 = 0.7938^{+0.0078}_{-0.0076}$ in CMB+BAO+DES-Y5. Our result is 1.49σ lower than $\sigma_8 = 0.819 \pm 0.015$ [34], which is provided by the combination of ACT DR6 lensing and BAO. Compared with $\sigma_8 = 0.8111 \pm 0.0060$ from Planck PR3 TTTEEE+lowE+lensing [8], the difference is 1.76σ . As for DES-Y3, the value of σ_8 is $0.783^{+0.073}_{-0.092}$ [35, 36] and the difference is 0.15σ . In [46], the CMB uses Planck 2018 PR3 TTTEEE ($l > 30$), Planck Commander likelihood TT ($2 \leq l \leq 30$), Planck SimAll likelihood EE ($2 \leq l \leq 30$) and a lensing likelihood combination of Planck PR4 and ACT-DR6. They also add DESI DR1 and DES-Y5. The result is $\sigma_8 = 0.8083 \pm 0.0086$. In comparison, our result is 1.25σ lower, effectively reducing the σ_8 tension and lowering the error bar by 10%. In general, the two sets of constraints maintain good consistency.

5. Feng-Shen-Li-Li parametrization

The next model we study is the Feng-Shen-Li-Li (FSLL) parametrization [47]. It has two cases:

$$\text{FSLL I: } w(a) = w_0 - w_a \frac{a(1-a)}{a^2 + (a-1)^2}, \quad (7)$$

$$\text{FSLI II : } w(a) = w_0 - w_a \frac{(a-1)^2}{a^2 + (a-1)^2}. \quad (8)$$

Corresponding $X(a)$ can be described as:

$$\text{FSLI I : } X(a) = a^{-3-3w_0} \text{Exp} \left[\frac{3}{8} w_a (\pi + 4 \arctan(1-2a) + 2 \ln(2a^2 - 2a + 1)) \right], \quad (9)$$

$$\text{FSLI II : } X(a) = a^{-3-3w_0-3w_a} \text{Exp} \left[-\frac{3}{8} w_a (\pi + 4 \arctan(1-2a) - 2 \ln(2a^2 - 2a + 1)) \right]. \quad (10)$$

The CPL model exhibits a divergence issue when the redshift z approaches -1, which undoubtedly represents a non-physical feature. This hinders the CPL parameterization from truly encompassing scalar field models and other theoretical models. The FSLI model overcomes this issue, extending the parameterization of dark energy to redshifts z approaching -1. When $z = -1$, FSLI I has $w(z) = w_0 - \frac{1}{2}w_a$, while FSLI II has $w(z) = w_0 + \frac{1}{2}w_a$, and when $z \ll 1$, FSLI I becomes linear, similar to the CPL model.

The DE EOS parameter constraints for FSLI I and FSLI II are very similar. The w_0 for both under CMB+BAO+DES-Y5 deviates from -1 at the 95% C.L.. Specifically, for FSLI I, $w_0 = -0.948^{+0.052}_{-0.050}$; for FSLI II, $w_0 = -0.945 \pm 0.048$. Figures 5 and 6 more intuitively demonstrate the consistency of the constraints between the two models. w_0 under CMB+BAO+PantheonPlus and CMB+BAO+Union3 also exhibits a non-smooth one-dimensional distribution, a feature previously observed in CPL and JBP.

We have strict constraints on DE EOS parameters. In comparison, [48] analyzes two forms of the FSLI model, using a combination of different BAO observations with $0.11 \leq z \leq 2.40$, CMB distant prior, the SNIa Pantheon, and the GRB dataset consisting of 162 measurements with $0.03351 \leq z \leq 9.3$. When only using CMB+BAO (hereinafter CB), FSLI I has $w_0 = -0.92 \pm 0.1$ and $w_a = 0.22 \pm 0.24$; FSLI II has $w_0 = -0.91 \pm 0.09$ and $w_a = 0.26 \pm 0.2$. When adding SNIa and GRB (hereinafter CBSG), the result of w_0 decreases, $w_0 = -1.06 \pm 0.04$ for FSLI I and $w_0 = -1.04 \pm 0.03$ for FSLI II; while the value of w_a increases, $w_a = 0.32 \pm 0.14$ for FSLI I and $w_a = 0.35 \pm 0.13$ for FSLI II. Our analysis for CMB+BAO+PantheonPlus, FSLI I has $w_0 = -0.971^{+0.009}_{-0.028}$, difference of 0.51σ with CB, 1.82σ with CBSG, $w_a = 0.004^{+0.030}_{-0.043}$, difference of 0.89σ with CB, 2.21σ with CBSG; while FSLI II has $w_0 = -0.968^{+0.011}_{-0.029}$ with a 0.64σ discrepancy to CB, 1.73σ to CBSG, and $w_a = -0.006^{+0.027}_{-0.036}$ with a 1.32σ discrepancy to CB, 2.68σ to CBSG. Obviously, CB is in better agreement with our results than CBSG, which may be due to the expansion of PantheonPlus and the influence of GRB.

The Planck PR3 shows the Hubble constant $H_0 = 67.36 \pm 0.54$ km/s/Mpc [8] and the local measurement gives $H_0 = 73.04 \pm 1.04$ km/s/Mpc [6]. When using the FSLI I model, $H_0 = 67.42^{+0.49}_{-0.40}$ km/s/Mpc in CMB+BAO+PantheonPlus, with a difference of 0.09σ to Planck PR3, 4.89σ to Local; $H_0 = 66.98^{+0.52}_{-0.51}$ km/s/Mpc in CMB+BAO+DES-Y5, with a difference of 0.51σ to Planck PR3, 5.21σ to Local; and $H_0 = 67.28^{+0.60}_{-0.46}$ km/s/Mpc in CMB+BAO+Union3, with a difference of 0.10σ to Planck PR3, 4.80σ to Local. Switching to the FSLI II model, $H_0 = 67.41^{+0.53}_{-0.41}$ km/s/Mpc in CMB+BAO+PantheonPlus differs by 0.07σ for Planck PR3, 4.82σ for Local; $H_0 = 66.90 \pm 0.53$ km/s/Mpc under CMB+BAO+DES-Y5 differs by 0.61σ for Planck PR3, 5.26σ for Local; and $H_0 = 67.20^{+0.67}_{-0.48}$ km/s/Mpc in CMB+BAO+Union3, with a difference of 0.19σ for Planck PR3, 4.72σ for Local. The H_0 tension of the two models under CMB+BAO+DES-Y5 both exceeds 5σ , the difference reaches the maximum value.

The σ_8 constraints derived from the two forms of the FSLI model are very similar. Therefore, in the following analysis, only the FSLI I model will be compared with other data results below. Planck PR3 showed $\sigma_8 = 0.8111 \pm 0.0060$ [8] and ACT DR6+BAO obtained $\sigma_8 = 0.819 \pm 0.015$ [34], while DES-Y3 gave the later σ_8 measurement value $\sigma_8 = 0.783^{+0.073}_{-0.092}$ [35, 36]. In our analysis, under CMB+BAO+PantheonPlus, $\sigma_8 = 0.7972^{+0.0078}_{-0.0072}$, the differences are 1.41σ for Planck PR3, 1.29σ for ACT DR6+BAO, 0.19σ for DES-Y3; under CMB+BAO+DES-Y5, $\sigma_8 = 0.7927 \pm 0.0080$, there are differences of 1.84σ for Planck PR3, 1.55σ for ACT DR6+BAO, 0.13σ for DES-Y3; finally, in CMB+BAO+Union3, $\sigma_8 = 0.7958^{+0.0084}_{-0.0070}$, with differences of 1.48σ for Planck PR3, 1.35σ for ACT DR6+BAO, 0.17σ for DES-Y3. We can see that the differences between our results and DES-Y3 have been controlled within 0.2σ , greatly reducing the σ_8 tension.

6. Barboza-Alcaniz parameterization

The Barboza-Alcaniz (BA) parameterization [49] is characterized by the form:

$$w(a) = w_0 + w_a \frac{1-a}{a^2 + (1-a)^2}. \quad (11)$$

$X(a)$ can be written as:

$$X(a) = a^{-3-3w_0-3w_a}(2a^2 - 2a + 1)^{\frac{3}{2}w_a}. \quad (12)$$

The DE EOS parameters of the BA model show the most significant variations, with w_0 being the largest across all three datasets. Specifically, under the CMB+BAO+DES-Y5, $w_0 = -0.892 \pm 0.095$; under the CMB+BAO+Union3, $w_0 = -0.882^{+0.144}_{-0.113}$, both of which can deviate from -1 at 99% C.L.. Meanwhile, for CMB+BAO+PantheonPlus, a deviation of -1 is also achieved at the 2σ level, with a value of $w_0 = -0.938^{+0.065}_{-0.060}$ at 95% C.L.. The divergence between the BA model and the Λ CDM model is the most significant among all DDE models. Figure 7 shows an inverse relationship between w_0 and w_a . w_a of the BA model is the minimum value of all DDE models in their corresponding datasets. Furthermore, the one-dimensional distribution plots show that under CMB+BAO+Union3 (blue line), the confidence intervals are significantly wider, so that the error bars are higher, indicating a relatively broader constraint effect.

Our constraints for DE EOS are $w_0 = -0.938^{+0.028}_{-0.040}$, $w_a = -0.047^{+0.041}_{-0.035}$ in CMB+BAO+PantheonPlus; $w_0 = -0.892 \pm 0.037$, $w_a = -0.095 \pm 0.041$ in CMB+BAO+DES-Y5; $w_0 = -0.882^{+0.051}_{-0.058}$, $w_a = -0.104^{+0.058}_{-0.057}$ in CMB+BAO+Union3. [50] also constrained the DE EOS parameters of the BA model. They used 14 BAO distance and expansion rate measurements from the SDSS-IV eBOSS, and combined them with three SNIa: PantheonPlus, DES-Y5 and Union3. Compared with our corresponding results, in PantheonPlus+BAO, $w_0 = -0.901 \pm 0.058$ with a 0.57σ difference and $w_a = -0.10^{+0.45}_{-0.37}$ with a 0.12σ difference; in DES-Y5+BAO, $w_0 = -0.962^{+0.031}_{-0.036}$ with a 1.45σ difference and $w_a = 0.06^{+0.43}_{-0.34}$ with a 0.45σ difference; in Union3+BAO, $w_0 = -0.768 \pm 0.080$ with a difference of 1.20σ and $w_a = -0.43^{+0.49}_{-0.39}$ with a difference of 0.66σ . This is in good agreement with our results. From the perspective of error bar, we have included CMB and updated BAO, which effectively strengthened the constraints and provided a lower error bar.

The BA model has the lowest H_0 values of all models, which maximizes the H_0 tension. Compared with the Planck PR3 value $H_0 = 67.36 \pm 0.54$ km/s/Mpc [8] and the local measurement $H_0 = 73.04 \pm 1.04$ km/s/Mpc [6], H_0 under CMB+BAO+PantheonPlus is $67.15^{+0.56}_{-0.50}$ km/s/Mpc, with a difference of 0.27σ for Planck PR3, 4.99σ for Local; H_0 under CMB+BAO+DES-Y5 is $66.47^{+0.55}_{-0.54}$ km/s/Mpc, with a difference of 1.15σ for Planck PR3, 5.58σ for Local; and H_0 under CMB+BAO+Union3 is $66.33^{+0.81}_{-0.78}$ km/s/Mpc, with a difference of 1.06σ for Planck PR3, 5.09σ for Local.

The σ_8 is clearly positively correlated with the H_0 , so the σ_8 value of the BA model is also the lowest among all models. We still compare it with Planck PR3: $\sigma_8 = 0.8111 \pm 0.0060$ [8], ACT DR6+BAO: $\sigma_8 = 0.819 \pm 0.015$ [34] and DES-Y3: $\sigma_8 = 0.783^{+0.073}_{-0.092}$ [35, 36]. Our results, under CMB+BAO+PantheonPlus, $\sigma_8 = 0.7951 \pm 0.0074$, with a difference of 1.68σ to Planck PR3, 1.43σ to ACT DR6+BAO, 0.16σ to DES-Y3; under CMB+BAO+DES-Y5, $\sigma_8 = 0.7892 \pm 0.0074$, a difference of 2.30σ to Planck PR3, 1.78σ to ACT DR6+BAO, 0.08σ to DES-Y3; and under CMB+BAO+Union3, $\sigma_8 = 0.7877 \pm 0.0093$, differs by 2.11σ to Planck PR3, 1.77σ to ACT DR6+BAO, 0.06σ to DES-Y3. Our data differed most from Planck PR3, followed by ACT DR6+BAO, as for DES-Y3, the differences can be completely negligible.

It is emphasized that among all two-parameter DDE models, the AIC value of the BA model is the smallest across all three datasets. In particular, when combined with CMB+BAO+DES-Y5, the AIC value is lower than the Λ CDM model and the one-parameter DDE model w CDM, indicating that the BA model will be more favored.

7. Logarithmic parametrization

Going a step further, the logarithmic (LOG) parametrization [51] is:

$$w(a) = w_0 - w_a \ln a. \quad (13)$$

We can also obtain:

$$X(a) = a^{-3-3w_0+\frac{3}{2}w_a \ln a}. \quad (14)$$

The constraints of DE EOS parameters for LOG model show the same trend as the BA model, but its performance is slightly weaker. Under CMB+BAO+PantheonPlus and CMB+BAO+Union3, w_0 deviates from -1 at 95% C.L., with values of $-0.955^{+0.052}_{-0.044}$ and $-0.931^{+0.075}_{-0.067}$, respectively. The difference is most significant in CMB+BAO+DES-Y5, $w_0 = -0.920^{+0.079}_{-0.073}$ at 99% C.L., deviating from -1 at the 3σ level. As can be seen in Fig. 8, there is a clear differentiation among the three datasets. The LOG model is highly sensitive to the use of datasets. Specifically, the peaks of the one-dimensional distribution graphs of the DE EOS parameters w_0 , w_a and the main cosmological parameters H_0 , Ω_m and σ_8 basically do not overlap, and the differentiation phenomenon is obvious.

We obtain the values of w_0 and w_a from three different datasets, in CMB+BAO+PantheonPlus, $w_0 = -0.955_{-0.034}^{+0.019}$ and $w_a = -0.028_{-0.031}^{+0.034}$; in CMB+BAO+DES-Y5, $w_0 = -0.920 \pm 0.031$ and $w_a = -0.063_{-0.039}^{+0.033}$; finally, in CMB+BAO+Union3, $w_0 = -0.931_{-0.048}^{+0.030}$ and $w_a = -0.052_{-0.039}^{+0.049}$. [45] also provides constraints on DE EOS parameters for the JBP model. When compared with our constraints, the specific results are as follows: in Planck 2018+DESI DR2+PantheonPlus, $w_0 = -0.887 \pm 0.050$, there is a 1.27σ difference, $w_a = -0.290_{-0.140}^{+0.180}$, there is a 1.43σ difference; in Planck 2018+DESI DR2+DES-SN5Y ($z > 0.01$), $w_0 = -0.876_{-0.092}^{+0.082}$, the difference is 0.45σ , $w_a = -0.320_{-0.190}^{+0.250}$, the difference is 1.02σ ; in Planck 2018+DESI DR2+Union3, $w_0 = -0.760 \pm 0.075$ with a 2.12σ difference, $w_a = -0.570_{-0.190}^{+0.230}$ with a 2.22σ difference. It can be seen that the differences in w_a between the three datasets are greater than those in w_0 . SNIa data is crucial. When using DES-Y5, the differences are the smallest and the fit is the highest; when using Union3, the differences are the largest, both exceeding 2σ .

The Hubble constant is 67.36 ± 0.54 km/s/Mpc from Planck PR3 [8] and the local measurement shows $H_0 = 73.04 \pm 1.04$ km/s/Mpc [6]. It exhibits distinct discrepancies with H_0 values derived from three different datasets: based on CMB+BAO+PantheonPlus, $H_0 = 67.28_{-0.44}^{+0.56}$ km/s/Mpc, it differs by 0.10σ to Planck PR3, 4.88σ to Local; based on CMB+BAO+DES-Y5, $H_0 = 66.67_{-0.53}^{+0.54}$ km/s/Mpc, by 0.90σ to Planck PR3, 5.44σ to Local; and for CMB+BAO+Union3 $H_0 = 66.86_{-0.61}^{+0.77}$ km/s/Mpc, with 0.53σ for Planck PR3, 4.78σ for Local. When the SNIa is DES-Y5, the H_0 tension is most significant.

Compared with $\Omega_m = 0.3153 \pm 0.0073$ from Planck PR3 [8], our constraint for CMB+BAO+PantheonPlus is $\Omega_m = 0.3098_{-0.0054}^{+0.0045}$, with the difference of 0.64σ ; for CMB+BAO+DES-Y5 is $\Omega_m = 0.3152 \pm 0.0052$, with the difference of 0.01σ ; for CMB+BAO+Union3 is $\Omega_m = 0.3136_{-0.0072}^{+0.0058}$, with a difference of 0.18σ . [52] also presents the Ω_m of the LOG model under the constraints of CMB and DESI DR2. The CMB uses Planck 2018 high- l TTTEEE, as well as the low- l likelihood for TT only and the low- l EE-only SimAll likelihood, incorporating the reconstructed lensing potential derived from the 3-point correlation function for Planck data [8, 53]. The constraint is $\Omega_m = 0.344_{-0.022}^{+0.016}$. Compared with our results from three datasets, the differences are 1.52σ , 1.27σ and 1.34σ , respectively. The three SNIa data that we added result in a difference of less than 2σ . The values of Ω_m in our analysis are closer to $\Omega_m = 0.290_{-0.063}^{+0.039}$ provided by DES-Y3 [35, 36], thus narrowing the gap. On the other hand, the error bar of our results also has a clear advantage.

The AIC value of the LOG model also shows certain advantages. Under CMB+BAO+DES-Y5, we find that the AIC is not only lower than the w CDM model but also lower compared to the Λ CDM model, indicating a preference for the LOG model.

8. Exponential parametrization

The exponential (EXP) parametrization [54, 55] has the following form:

$$w(a) = w_0 + w_a [\text{Exp}(1 - a) - 1]. \quad (15)$$

We can get its $X(a)$ as:

$$X(a) = a^{-3-3w_0+3w_a} \text{Exp}[3ew_a(Ei(-1) - Ei(-a))]. \quad (16)$$

Here $Ei(x) = -\int_{-x}^{\infty} \frac{e^{-x}}{x} dx$ (for $x < 0$) is the exponential integral function.

We can find in Fig. 9 that the EXP model exhibits strong constraining capabilities compared to other models, particularly in terms of constraining the DE EOS parameters w_0 and w_a . In CMB+BAO+PantheonPlus, $w_0 = -0.971_{-0.016}^{+0.012}$, $w_a = -0.011_{-0.016}^{+0.014}$; In CMB+BAO+DES-Y5, $w_0 = -0.956_{-0.014}^{+0.013}$, $w_a = -0.029_{-0.015}^{+0.013}$; and for CMB+BAO+Union3, we can get $w_0 = -0.958_{-0.019}^{+0.017}$, $w_a = -0.026_{-0.019}^{+0.020}$. It can be seen that the ranges of 68% confidence interval for EXP model are the smallest in the corresponding datasets.

Similarly to the BA model, the w_0 of the EXP model also differs significantly from the Λ CDM model. Under CMB+BAO+DES-Y5 and CMB+BAO+Union3, w_0 deviates from -1 at the 99% C.L., with values of $-0.956_{-0.034}^{+0.040}$ and $-0.958_{-0.041}^{+0.047}$, respectively. Under CMB+BAO+PantheonPlus, the difference decreases slightly, with w_0 deviating from -1 at the 2σ level, $w_0 = -0.971_{-0.026}^{+0.027}$ at 95% C.L..

Our three datasets have strong constraints on DE EOS parameters of the EXP model. In comparison, [52] also gives the results of w_0 and w_a for the EXP model under the joint constraints of CMB and DESI DR2. The results are $w_0 = -0.51_{-0.22}^{+0.17}$ and $w_a = -1.19_{-0.57}^{+0.55}$. Compared to our results, under CMB+BAO+PantheonPlus, w_0 differs by 2.09σ and w_a differs by 2.14σ ; under CMB+BAO+DES-Y5, w_0 has a 2.02σ difference and w_a has a 2.11σ difference; in the end, under CMB+BAO+DES-Y5, w_0 has a discrepancy of 2.03σ and w_a has a discrepancy of 2.12σ . We can

see that the differences in w_a under the three datasets are slightly greater than w_0 , and all are concentrated around 2σ . This difference is mainly due to the SNIa data we added.

The Hubble constant H_0 is 67.36 ± 0.54 km/s/Mpc under Planck PR3 constraints [8] and 73.04 ± 1.04 km/s/Mpc under local measurements [6]. Our results, specifically, for the $H_0 = 67.25^{+0.58}_{-0.57}$ km/s/Mpc derived from CMB+BAO+PantheonPlus, the differences are 0.14σ for Planck PR3 and 4.86σ for Local; for the $H_0 = 66.54 \pm 0.56$ km/s/Mpc obtained from CMB+BAO+DES-Y5, the differences are 1.05σ for Planck PR3 and 5.50σ for Local; for the $H_0 = 66.66^{+0.80}_{-0.78}$ km/s/Mpc from CMB+BAO+Union3, the differences are 0.73σ for Planck PR3 and 4.86σ for Local.

We show the value of Ω_m from Planck PR3: $\Omega_m = 0.3153 \pm 0.0073$ [8]. When comparing our results with this value, we find that the divergences of Ω_m are 0.57σ in CMB+BAO+PantheonPlus, 0.14σ in CMB+BAO+DES-Y5 and 0.02σ in CMB+BAO+Union3. We can also see the constraints of Ω_m in Planck+DESI+PantheonPlus and Planck+DESI+DESY5 [46]. The former gives $\Omega_m = 0.3088 \pm 0.0067$, while the latter is slightly larger, $\Omega_m = 0.3157 \pm 0.0066$. Compared with our data, in CMB+BAO+PantheonPlus, $\Omega_m = 0.3102^{+0.0052}_{-0.0058}$, the difference is 0.16σ ; in CMB+BAO+DES-Y5, $\Omega_m = 0.3166 \pm 0.0055$, the difference is 0.10σ . The results show excellent consistency, with negligible differences, indicating that the updates to Planck PR4 and DESI DR2 have minimal impact on the influence of Ω_m to the EXP model.

The AIC values of the EXP model in CMB+BAO+PantheonPlus and CMB+BAO+Union3 are slightly higher. However, in CMB+BAO+DES-Y5, the AIC value is lower than the Λ CDM model, indicating that the EXP model is more favored.

The differences mentioned above are mainly due to significant updates and expansions to the datasets, which enhance the constraints on the models and alter the posterior distribution of the parameter space in various ways. Firstly, the update to CMB NPIPE (PR4) CamSpec is reflected. NPIPE is a new independent pipeline that offers substantial improvements in detector calibration and system correction compared to previous versions. Its low noise allows for tighter parameter constraints, and due to improved polarization, most Λ CDM parameters in TTTEEE have also improved by approximately 10% [30]. Secondly, updates to DESI DR2 have also played a crucial role. Compared to DESI DR1, the effective data volume has more than doubled and the statistical accuracy has also been improved. With more than 30 million redshifts for galaxies and quasars, and Ly α forest spectra for over 820,000 quasars, DESI DR2 represents the largest spectroscopic galaxy sample to date and provides the most precise BAO measurements at any redshift [12].

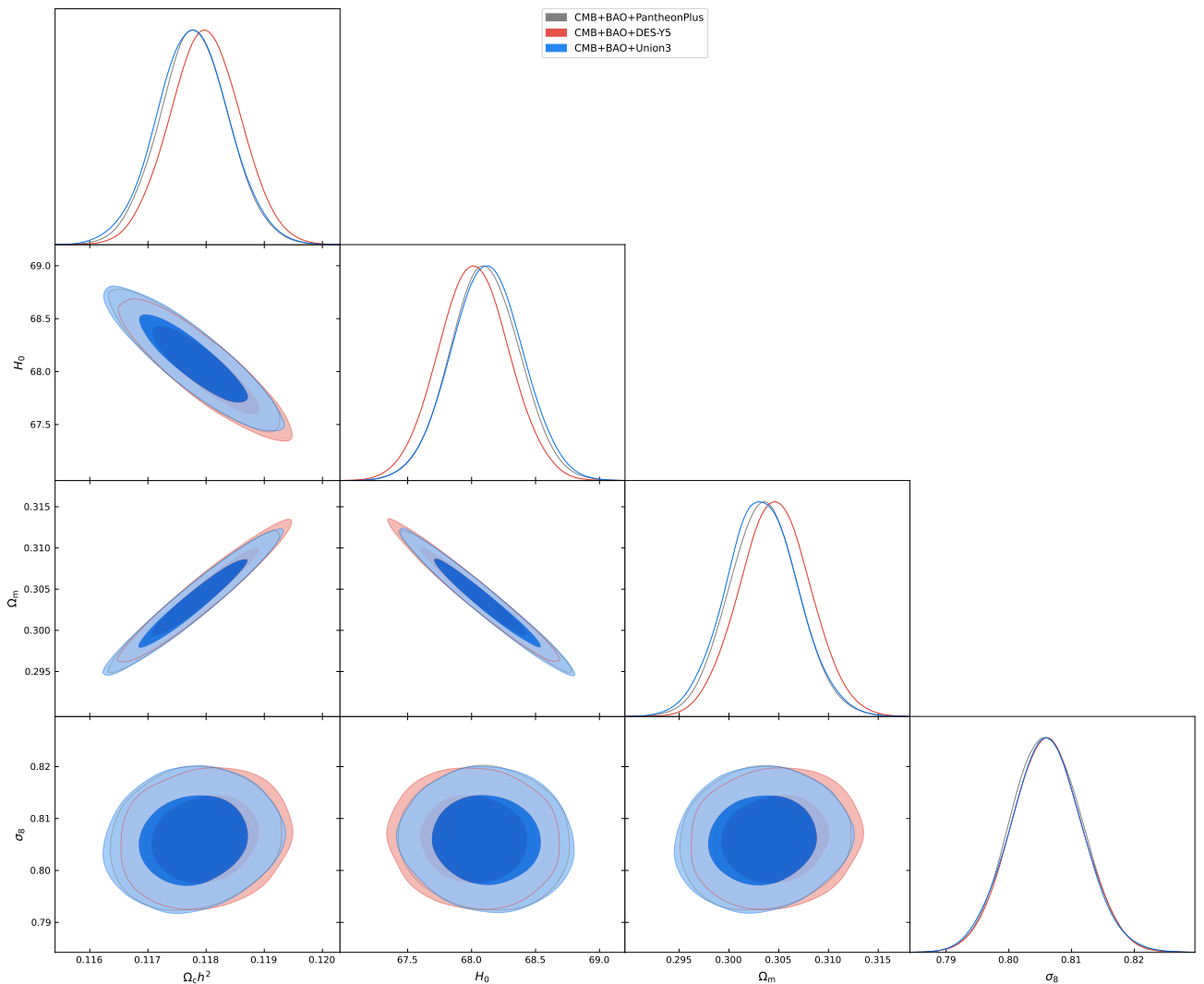


FIG. 1: The one-dimensional posterior distributions and two-dimensional marginalized contours for the main key parameters of the Λ CDM, derived from the dataset combinations of CMB+BAO+PantheonPlus, CMB+BAO+ DES-Y5 and CMB+BAO+Union3.

V. DISCUSSION

We will discuss from the following three perspectives:

Firstly, we discuss the changes in parameters when using different datasets under the same model.

1. In CMB+BAO+DES-Y5, there are differences in $\Omega_c h^2$ between the Λ CDM and w CDM models: the $\Omega_c h^2$ of the former is relatively high while the $\Omega_c h^2$ of the latter is lower. Then we discuss the parameters in w CDM, CPL, JBP, and FSLM models: the w_0 and Ω_m are larger, while the H_0 , and σ_8 are relatively small. The above models are very close under the constraints of CMB+BAO+PantheonPlus and CMB+BAO+Union3. The reason for this discrepancy may be related to the overlap in three SNIa datasets. Among the 2087 samples compiled by Union3, 1363 samples are identical to the samples in the PantheonPlus dataset [10]. The high degree of sample overlap makes the final constraints of the two datasets relatively close. The DES-Y5 dataset has only 194 low-redshift samples in common with the PantheonPlus [10], the number of overlaps is significantly smaller. Therefore, its constraints differ more from those of PantheonPlus.

2. In contrast, when the CMB+BAO+PantheonPlus dataset is used with the BA, LOG, and EXP models, the trend of parameters is reversed. Here, w_0 and Ω_m are lead to lower values, while H_0 and σ_8 are driven to higher values. CMB+BAO+DES-Y5 and CMB+BAO+Union3 provide similar constraints for the BA and EXP models, while LOG

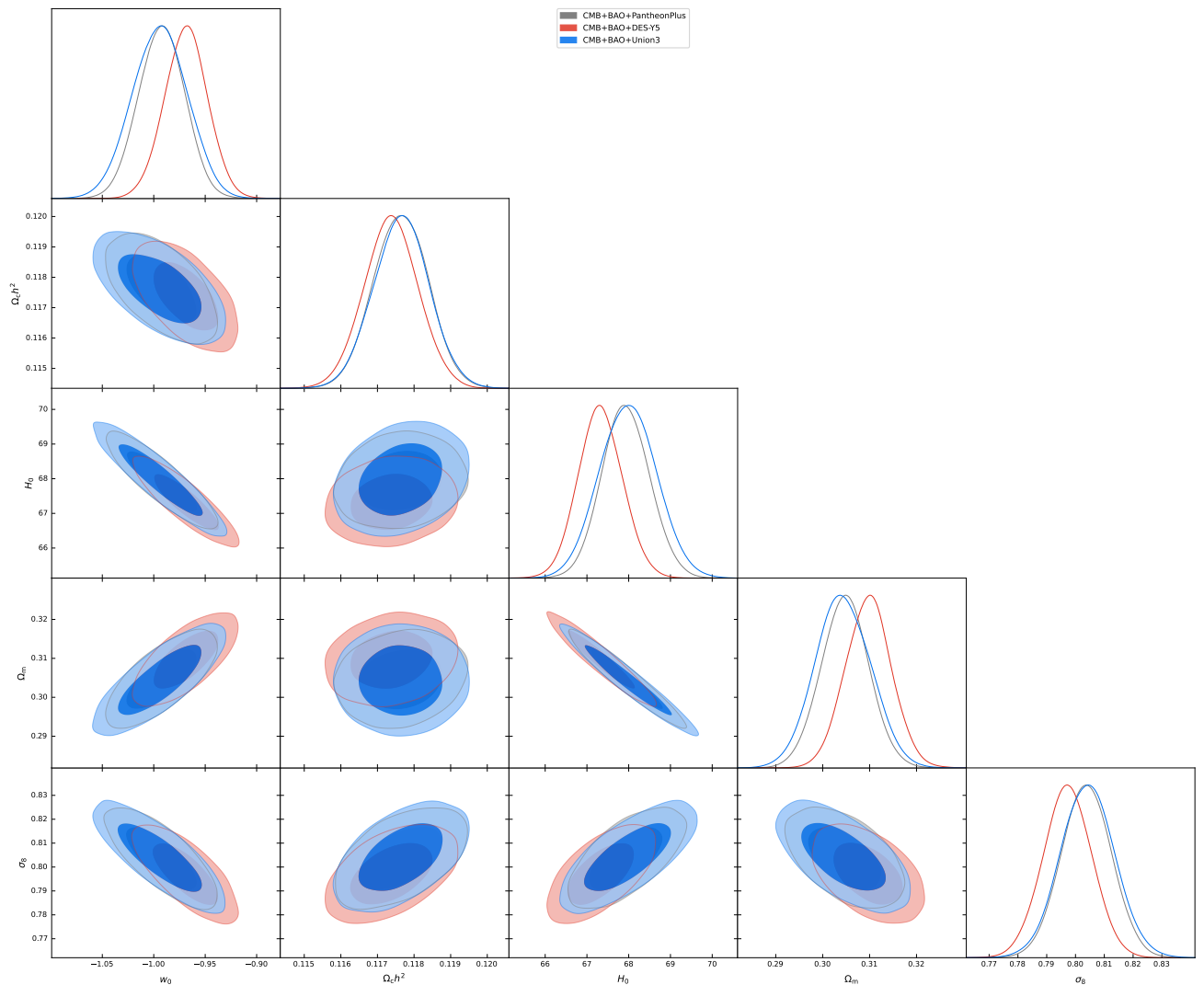


FIG. 2: The one-dimensional posterior distributions and two-dimensional marginalized contours for the main key parameters of the w CDM, derived from the dataset combinations of CMB+BAO+PantheonPlus, CMB+BAO+ DES-Y5 and CMB+BAO+Union3.

model shows clear differentiation between the three datasets. It is worth noting that the error bar of the results in CMB+BAO+Union3 is relatively large, indicating that its constraint capability is inferior to the other two datasets. 3. The H_0 values of all DDE models are smaller than Λ CDM, which is not helpful to alleviate the Hubble tension [5]. However, we find that the σ_8 values of all DDE models are smaller than Λ CDM, which is of positive significance for alleviating σ_8 tension. The most significant improvement comes from the BA model under the CMB+BAO+Union3 dataset.

Secondly, taking a different approach, we examine the trends in various parameters in different models using the same dataset.

1. In the CMB+BAO+PantheonPlus dataset, w_0 is significantly larger in the BA and LOG models, with the BA value being higher than the LOG value. In CPL, JBP, FSLL I and FSLL II models, the w_0 exhibit a nonsmooth one-dimensional posterior distribution, suggesting a possible multimodal structure in their parameter space. However, when we change SNIa to DES-Y5, the one-dimensional posterior distribution of w_0 for all models shows a smooth unimodal characteristic, indicating a significantly improved convergence in the parameter space.

2. The degree of deviation for w_0 from the standard value -1 in different models may be related to the SNIa data. Under CMB+BAO+PantheonPlus, only the BA, LOG, and EXP models deviate from -1 at 95% C.L.. When SNIa is replaced with Union3, the LOG model remains unchanged, but the BA and EXP models can deviate from -1 at

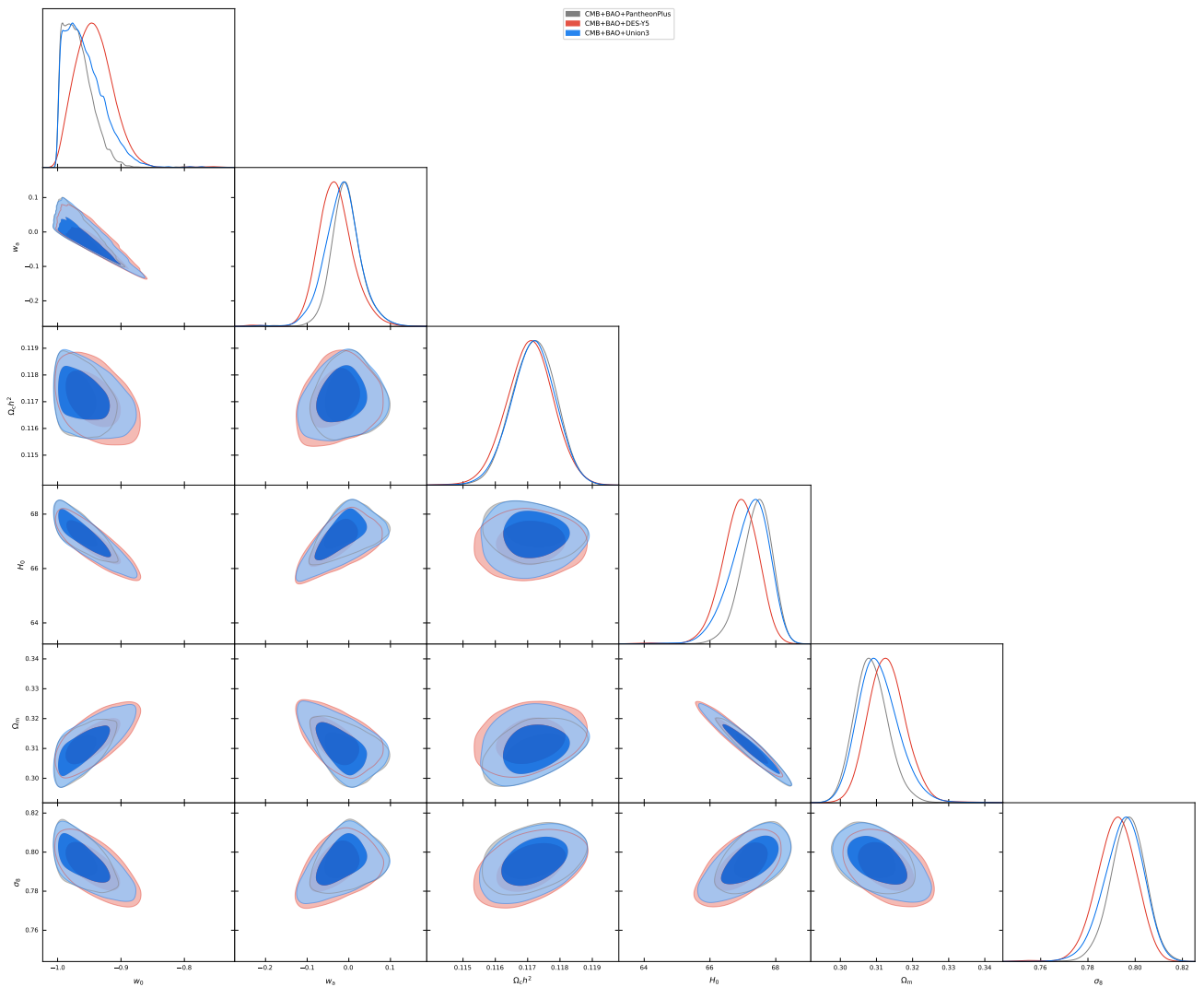


FIG. 3: The one-dimensional posterior distributions and two-dimensional marginalized contours for the main key parameters of the CPL, derived from the dataset combinations of CMB+BAO+PantheonPlus, CMB+BAO+ DES-Y5 and CMB+BAO+Union3.

99% C.L.. Finally, when using DES-Y5, the situation changes significantly. The w CDM model can deviate from -1 at 68% C.L.; CPL, JBP, and FSLM models can also deviate from -1 at 95% C.L.; while BA, LOG, and EXP models can all achieve deviation from -1 at 99% C.L.. From another perspective, the BA, LOG, and EXP models have larger differences from the Λ CDM model, and their obtained DDE evidence is more significant. The CPL, JBP, and FSLM models differ less from the Λ CDM model and can only obtain a certain preference for DDE. Finally, the w CDM model has the smallest difference compared to the Λ CDM model, and it is difficult to obtain sufficient DDE evidence, which is also consistent with its positioning as the smallest extension of the standard model.

3. We also analyze the impact of the three datasets on H_0 tension. Under the constraints of CMB+BAO+DES-Y5, the H_0 tension of all DDE models reached the maximum value among the three datasets. With the exception of the w CDM model, the H_0 tension of all models exceeded 5σ . Switching from SNIa to PantheonPlus improved the situation, with H_0 tension of all models decreasing and falling below 5σ . Finally, using the Union3 data further improved the situation, with the H_0 tension of most DDE models (except the BA and EXP models) reaching the lowest values among the three datasets. This suggests that using the DES-Y5 data may increase H_0 tension compared to PantheonPlus and Union3.

4. When using the CMB+BAO+Union3 dataset, the overall distribution of model parameters remains stable. Only σ_8 is relatively low in the BA, EXP and LOG models and exhibits an increasing trend.

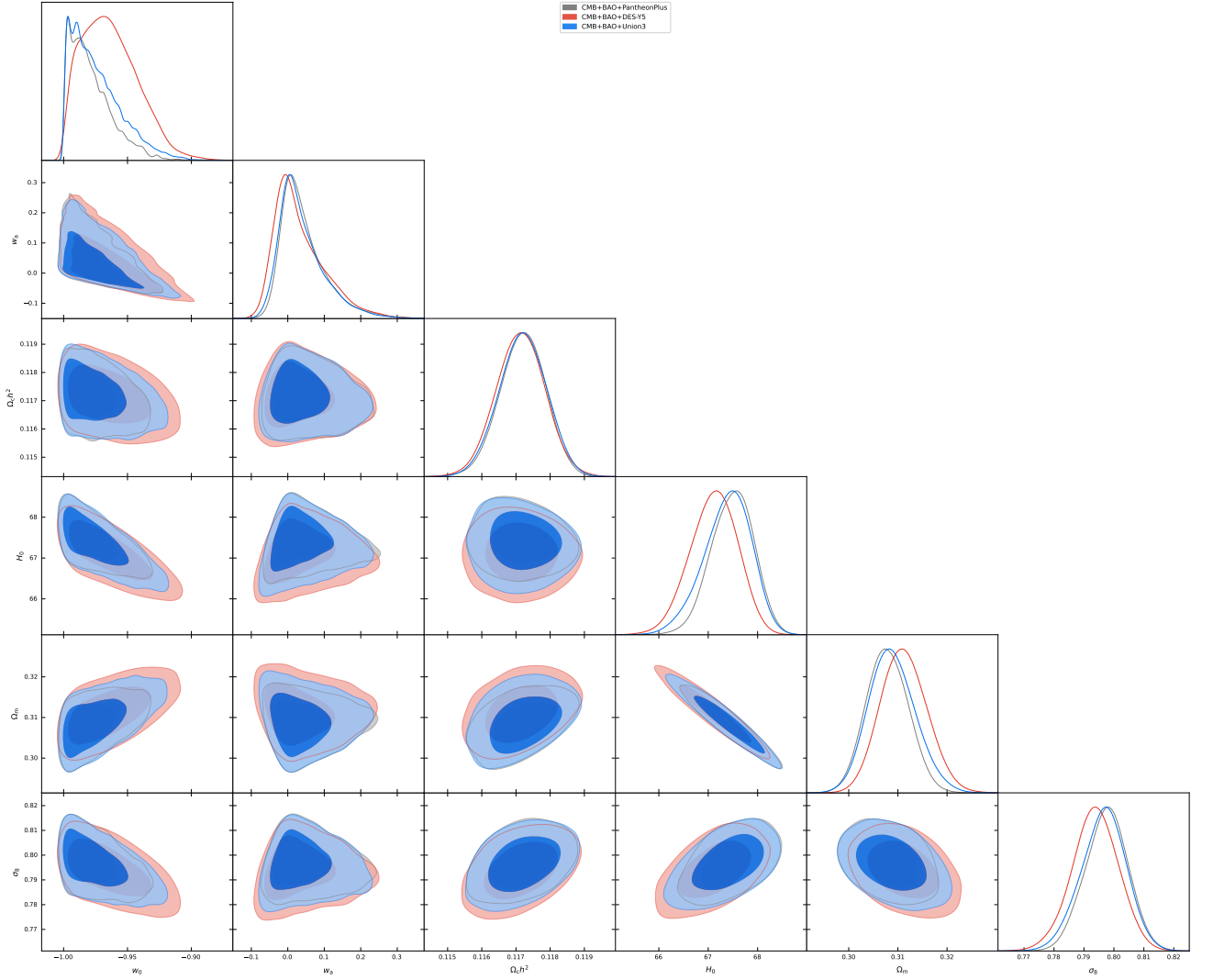


FIG. 4: The one-dimensional posterior distributions and two-dimensional marginalized contours for the main key parameters of the JBP, derived from the dataset combinations of CMB+BAO+PantheonPlus, CMB+BAO+ DES-Y5 and CMB+BAO+Union3.

Lastly, to compare the performance differences between various DDE models and the Λ CDM model, it is important to consider the additional parameters involved. The w CDM model has one additional degree of freedom w_0 , while other DDE models are two-parameter models, each with two additional degrees of freedom, w_0 and w_a . In this work, we use the AIC to appropriately penalize the presence of these additional parameters and demonstrate the degree of fit for all models to different observational combinations.

1. In the CMB+BAO+PantheonPlus datasets, the AIC values of the FSLL II, BA, LOG and EXP models are lower than the CPL model. This indicates that compared with the CPL model, the FSLL II, BA, LOG, and EXP models remain more favorable.
2. For the CMB+BAO+Union3 datasets, the FSLL II, BA, LOG, and EXP models also have lower AIC values than the CPL model. Moreover, the AIC value of the BA model is smaller than that of the w CDM model, which shows a certain superiority.
3. Then, let us focus on the CMB+BAO+DES-Y5 datasets. The FSLL II model still has a slight advantage in the AIC value over the CPL model. Meanwhile, the BA, LOG, and EXP models have made significant progress and generated more favorable evidence. All three models have lower AIC values than the CPL, w CDM, and Λ CDM models, especially compared to the Λ CDM model, which has gained more positive favor.

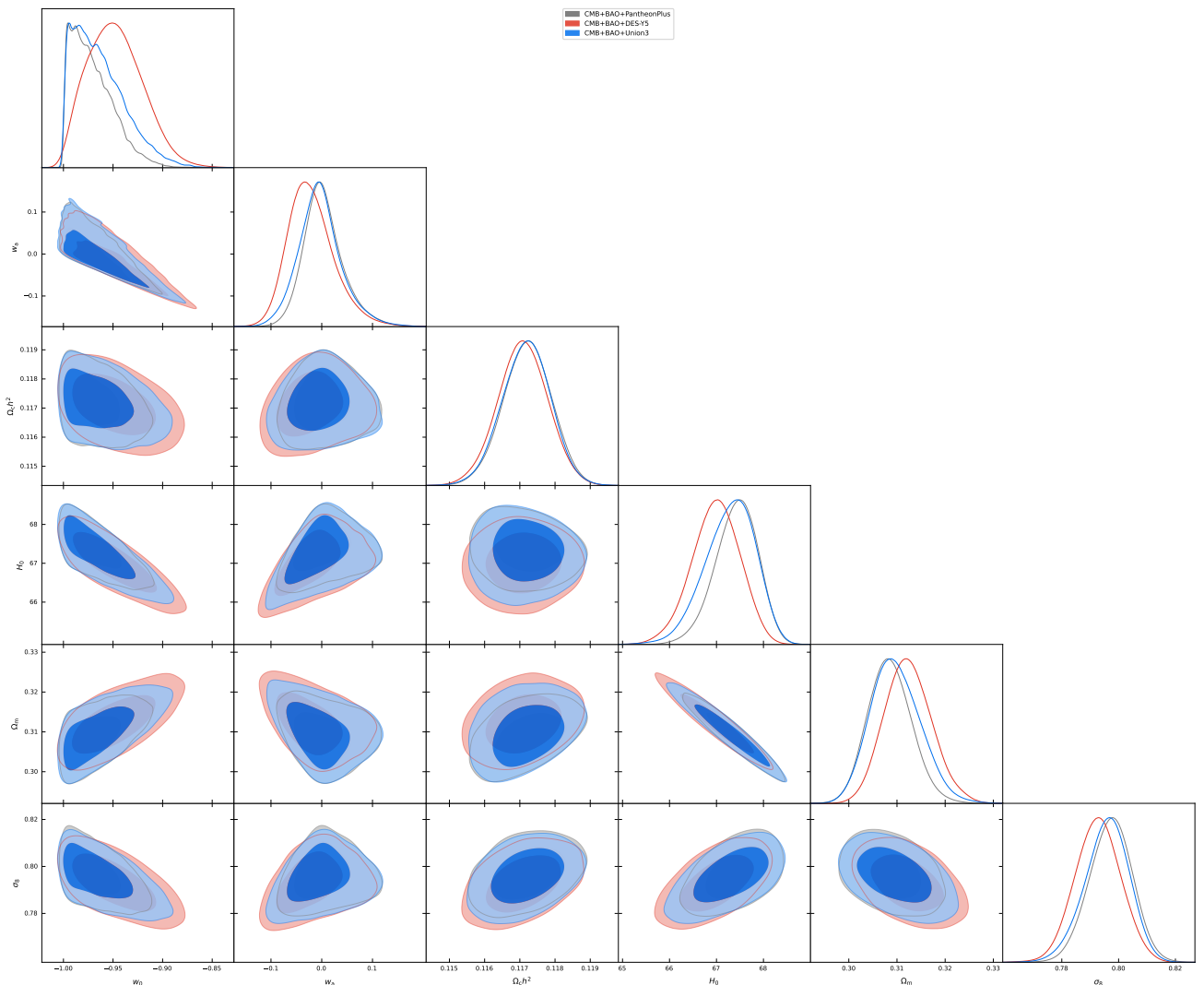


FIG. 5: The one-dimensional posterior distributions and two-dimensional marginalized contours for the main key parameters of the FSLI I, derived from the dataset combinations of CMB+BAO+PantheonPlus, CMB+BAO+ DES-Y5 and CMB+BAO+Union3.

4. We find that the AIC value of the BA model has a certain advantage in any dataset, being the minimum value among all two-parameter DDE models, which fully demonstrates the strong fitting ability of the BA model to these observational data.

VI. SUMMARY

In this paper, we analyze the Λ CDM model and DDE parameterized models, placing strict constraints on key cosmological parameters using three datasets: CMB+BAO+PantheonPlus, CMB+BAO+DES-Y5 and CMB+BAO+Union3. This completes a systematic survey.

The study performed a comparative analysis based on Λ CDM model, including the single-parameter DDE model: w CDM, and six two-parameter DDE models: CPL, JBP, FSLI, BA, LOG, and EXP. Our work focuses on the DE EOS parameters w_0 and w_a , while also constraining the important derived parameters H_0 , σ_8 and Ω_m . In particular, we put emphasis on H_0 tension. To ensure the timeliness and reliability of the analysis, our CMB data include Planck PR3 TTEE+lowE and the newly released Planck PR4 CamSpec high- l TTTEEE. For the BAO data, DESI DR2 is also used. Finally, three SNIa datasets are combined: PantheonPlus, DES-Y5 and Union3.

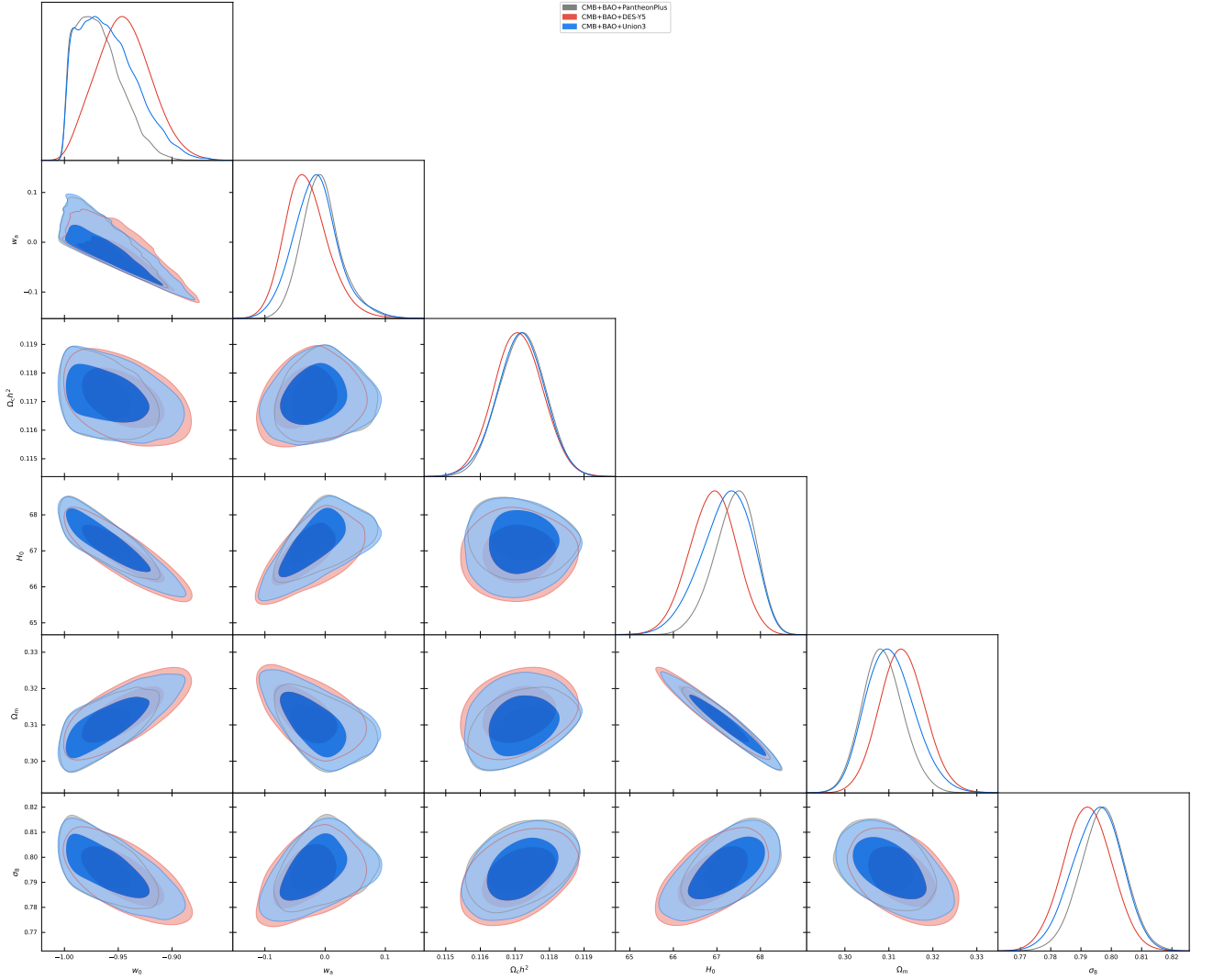


FIG. 6: The one-dimensional posterior distributions and two-dimensional marginalized contours for the main key parameters of the FSLI II, derived from the dataset combinations of CMB+BAO+PantheonPlus, CMB+BAO+ DES-Y5 and CMB+BAO+Union3.

Our analysis integrates the relatively scattered results in the field. Through a unified framework and standards, we compare the characteristics and advantages of different models and datasets, highlighting the systematicness and comprehensiveness of the research. Based on the above analysis, we find that while the Λ CDM model still dominates in the CMB+BAO+PantheonPlus and CMB+BAO+Union3 datasets, some DDE models (particularly BA, LOG and EXP) are positively favored over the Λ CDM model when combined with the CMB+BAO+DES-Y5 dataset. Among them, the BA model exhibits the strongest fitting ability, with its AIC value having a prominent advantage in all datasets. Meanwhile, we conclude that CMB+BAO+DES-Y5 significantly improves the convergence of the parameter space, resulting in smooth and unimodal posterior distributions for the w_0 parameter in all models. Furthermore, it increases w_0 and Ω_m , while decreasing H_0 and σ_8 in the w CDM, CPL, JBP and FSLI models. The BA, LOG, and EXP models exhibit the opposite trend when using CMB+BAO+PantheonPlus. This clearly demonstrates that the choice of dataset can significantly influence the estimated parameters of cosmological models. It should be mentioned that the use of DES-Y5 can exacerbate H_0 tension. This discovery provides a new reference for understanding the contradictions in the current Hubble constant measurement.

In the end, our findings offer inspiration for further in-depth research. Specifically, they encourage an exploration of the physical mechanisms for high-performance parameterized models such as BA, LOG, and EXP. Furthermore, this research can help explore why the parameters of these models can better fit to specific datasets. This may

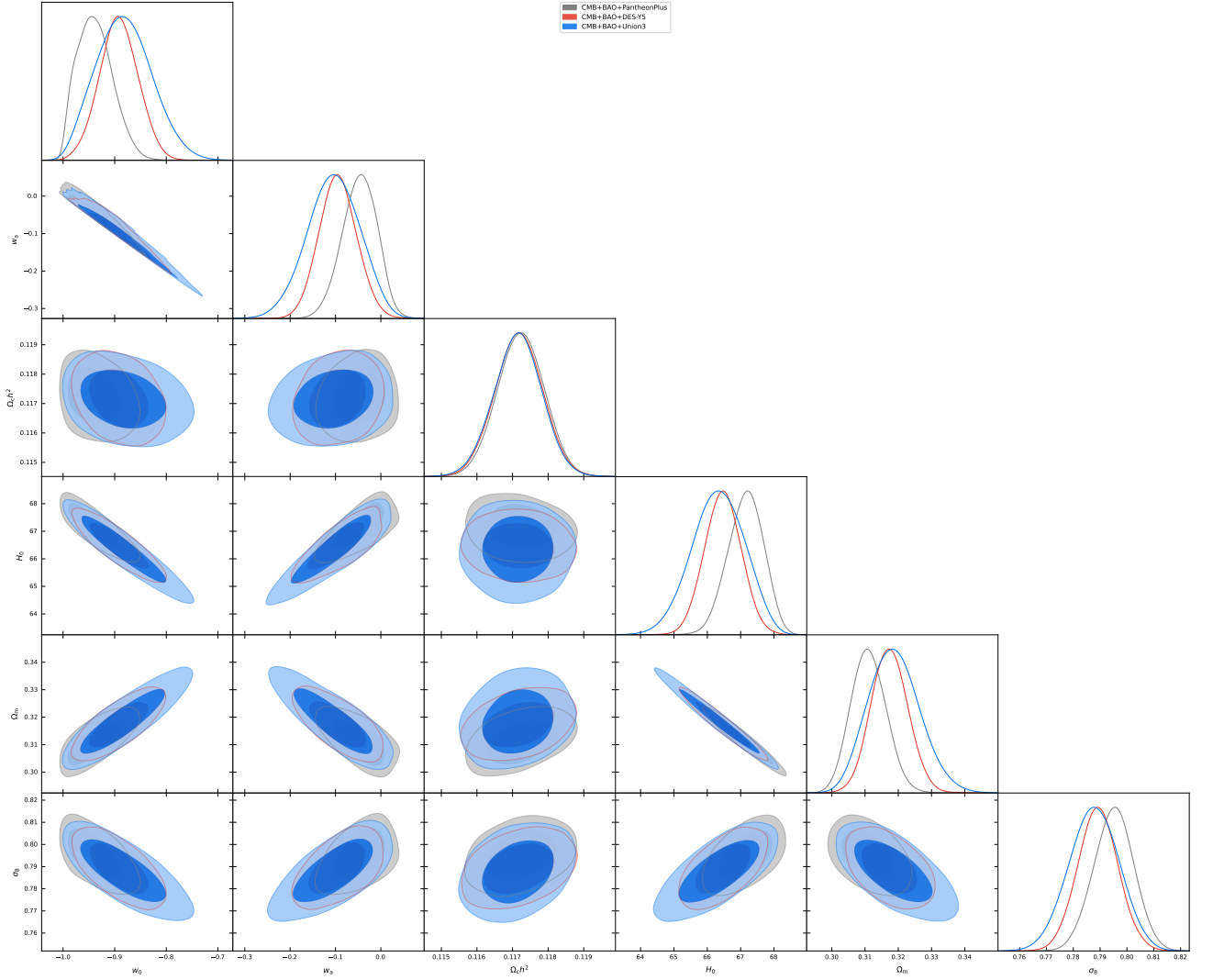


FIG. 7: The one-dimensional posterior distributions and two-dimensional marginalized contours for the main key parameters of the BA, derived from the dataset combinations of CMB+BAO+PantheonPlus, CMB+BAO+ DES-Y5 and CMB+BAO+Union3.

provide new theoretical clues for revealing the essence of dark energy.

Acknowledgments

We acknowledge the use of HPC Cluster of Tianhe II in National Supercomputing Center in Guangzhou. Lu Chen is supported by grants from NSFC (grant No. 12105164). This work has also received funding from project ZR2021QA021 supported by Shandong Provincial Natural Science Foundation and the Youth Innovation Team Plan of Colleges and Universities in Shandong Province (2023KJ350).

-
- [1] A. G. Riess *et al.* [Supernova Search Team], *Astron. J.* **116** (1998), 1009-1038 doi:10.1086/300499 [arXiv:astro-ph/9805201 [astro-ph]].
 - [2] S. Perlmutter *et al.* [Supernova Cosmology Project], *Astrophys. J.* **517** (1999), 565-586 doi:10.1086/307221 [arXiv:astro-ph/9812133 [astro-ph]].

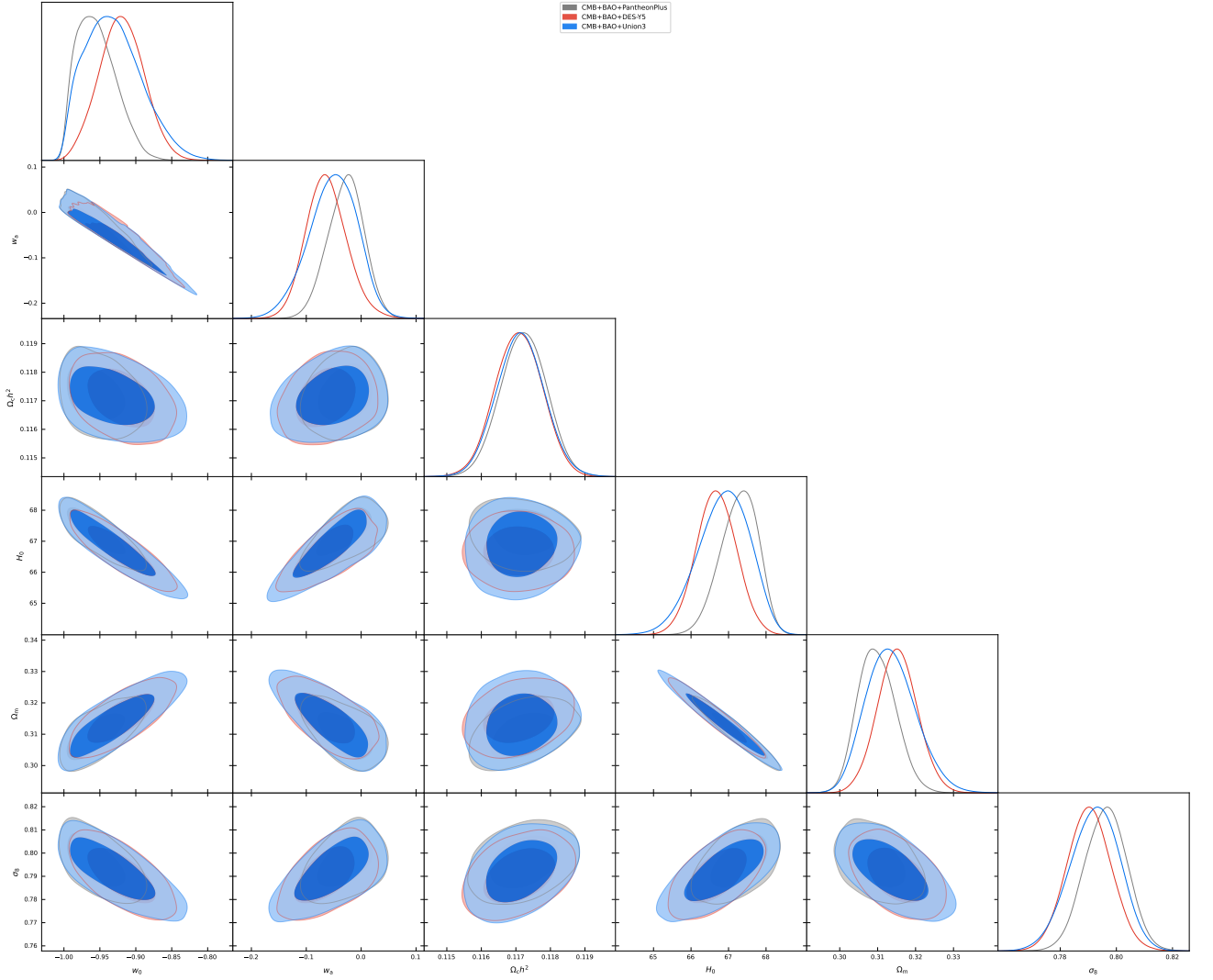


FIG. 8: The one-dimensional posterior distributions and two-dimensional marginalized contours for the main key parameters of the LOG, derived from the dataset combinations of CMB+BAO+PantheonPlus, CMB+BAO+ DES-Y5 and CMB+BAO+Union3.

TABLE III: The 68% limits for the cosmological parameters in the Λ CDM+ $\alpha/\alpha_{\text{EM}}$ and Λ CDM+ $\alpha_{\text{rec}}/\alpha_{\text{EM}}$ + $\alpha_{\text{rei}}/\alpha_{\text{EM}}$ model.

	Λ CDM+ $\alpha/\alpha_{\text{EM}}$	Λ CDM+ $\alpha_{\text{rec}}/\alpha_{\text{EM}}$ + $\alpha_{\text{rei}}/\alpha_{\text{EM}}$
$\Omega_b h^2$	0.02244 ± 0.00014	0.02241 ± 0.00014
$\Omega_c h^2$	0.1191 ± 0.0013	0.1198 ± 0.0013
$100\theta_{\text{MC}}$	1.04107 ± 0.00272	$1.04305^{+0.00280}_{-0.00284}$
$\ln(10^{10} A_s)$	3.0484 ± 0.0057	$3.0492^{+0.0064}_{-0.0068}$
n_s	$0.9670^{+0.0063}_{-0.0064}$	0.9630 ± 0.0064
$a_p [\text{M}_{\odot} \cdot \text{yr}^{-1} \cdot \text{Mpc}^{-3}]$	$0.01772^{+0.00070}_{-0.00071}$	$0.01633^{+0.00070}_{-0.00071}$
b_p	2.968 ± 0.121	$2.897^{+0.124}_{-0.134}$
c_p	$2.554^{+0.088}_{-0.101}$	$2.736^{+0.098}_{-0.112}$
d_p	5.125 ± 0.097	5.791 ± 0.140
$\alpha/\alpha_{\text{EM}}$	$1.000042^{+0.001983}_{-0.001972}$	-
$\alpha_{\text{rec}}/\alpha_{\text{EM}}$	-	$1.001494^{+0.002041}_{-0.002063}$
$\alpha_{\text{rei}}/\alpha_{\text{EM}}$	-	$0.854034^{+0.031678}_{-0.027209}$
τ	$0.0573^{+0.0005}_{-0.0006}$	$0.0559^{+0.0069}_{-0.0076}$
$10^4 Q_{\text{HII}}(z=22)$	2.133 ± 0.019	2.125 ± 0.020
$H_0 [\text{km} \cdot \text{s}^{-1} \cdot \text{Mpc}^{-1}]$	67.80 ± 0.67	68.17 ± 0.70

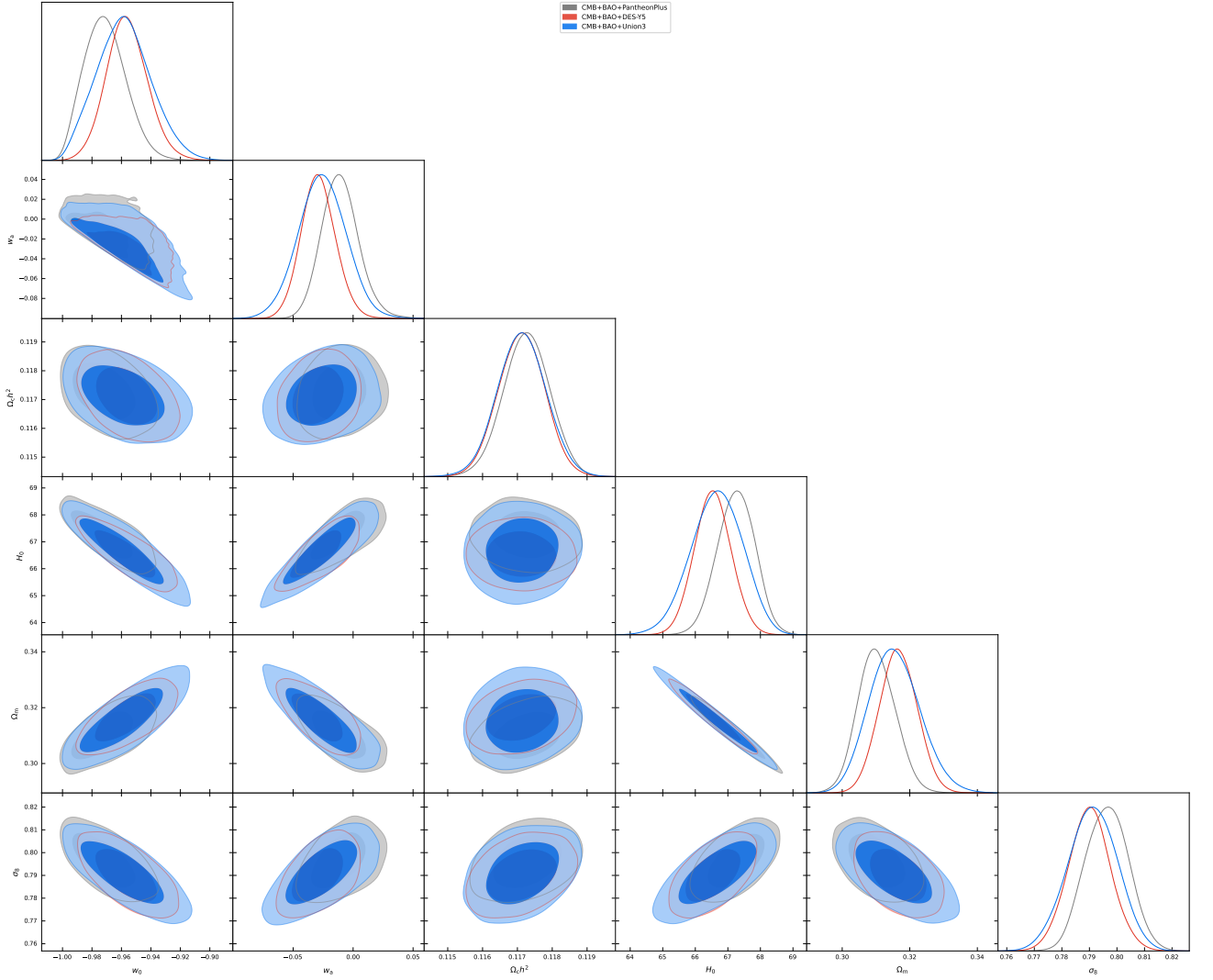


FIG. 9: The one-dimensional posterior distributions and two-dimensional marginalized contours for the main key parameters of the EXP, derived from the dataset combinations of CMB+BAO+PantheonPlus, CMB+BAO+ DES-Y5 and CMB+BAO+Union3.

- [3] K. Bamba, S. Capozziello, S. Nojiri and S. D. Odintsov, *Astrophys. Space Sci.* **342** (2012), 155-228 doi:10.1007/s10509-012-1181-8 [arXiv:1205.3421 [gr-qc]].
- [4] L. Verde, T. Treu and A. G. Riess, *Nature Astron.* **3** (2019), 891 doi:10.1038/s41550-019-0902-0 [arXiv:1907.10625 [astro-ph.CO]].
- [5] E. Di Valentino, O. Mena, S. Pan, L. Visinelli, W. Yang, A. Melchiorri, D. F. Mota, A. G. Riess and J. Silk, *Class. Quant. Grav.* **38** (2021) no.15, 153001 doi:10.1088/1361-6382/ac086d [arXiv:2103.01183 [astro-ph.CO]].
- [6] A. G. Riess, W. Yuan, L. M. Macri, D. Scolnic, D. Brout, S. Casertano, D. O. Jones, Y. Murakami, L. Breuval and T. G. Brink, *et al.* *Astrophys. J. Lett.* **934** (2022) no.1, L7 doi:10.3847/2041-8213/ac5c5b [arXiv:2112.04510 [astro-ph.CO]].
- [7] P. J. Wu and X. Zhang, *Phys. Rev. D* **112** (2025) no.6, 063514 doi:10.1103/sn3q-q589 [arXiv:2411.06356 [astro-ph.CO]].
- [8] N. Aghanim *et al.* [Planck], *Astron. Astrophys.* **641** (2020), A6 [erratum: *Astron. Astrophys.* **652** (2021), C4] doi:10.1051/0004-6361/201833910 [arXiv:1807.06209 [astro-ph.CO]].
- [9] A. Sousa-Neto, C. Bengaly, J. E. Gonzalez and J. Alcaniz, [arXiv:2502.10506 [astro-ph.CO]].
- [10] A. G. Adame *et al.* [DESI], *JCAP* **02** (2025), 021 doi:10.1088/1475-7516/2025/02/021 [arXiv:2404.03002 [astro-ph.CO]].
- [11] R. Calderon *et al.* [DESI], *JCAP* **10** (2024), 048 doi:10.1088/1475-7516/2024/10/048 [arXiv:2405.04216 [astro-ph.CO]].
- [12] M. Abdul Karim *et al.* [DESI], [arXiv:2503.14738 [astro-ph.CO]].
- [13] K. Lodha *et al.* [DESI], *Phys. Rev. D* **111** (2025) no.2, 023532 doi:10.1103/PhysRevD.111.023532 [arXiv:2405.13588 [astro-ph.CO]].

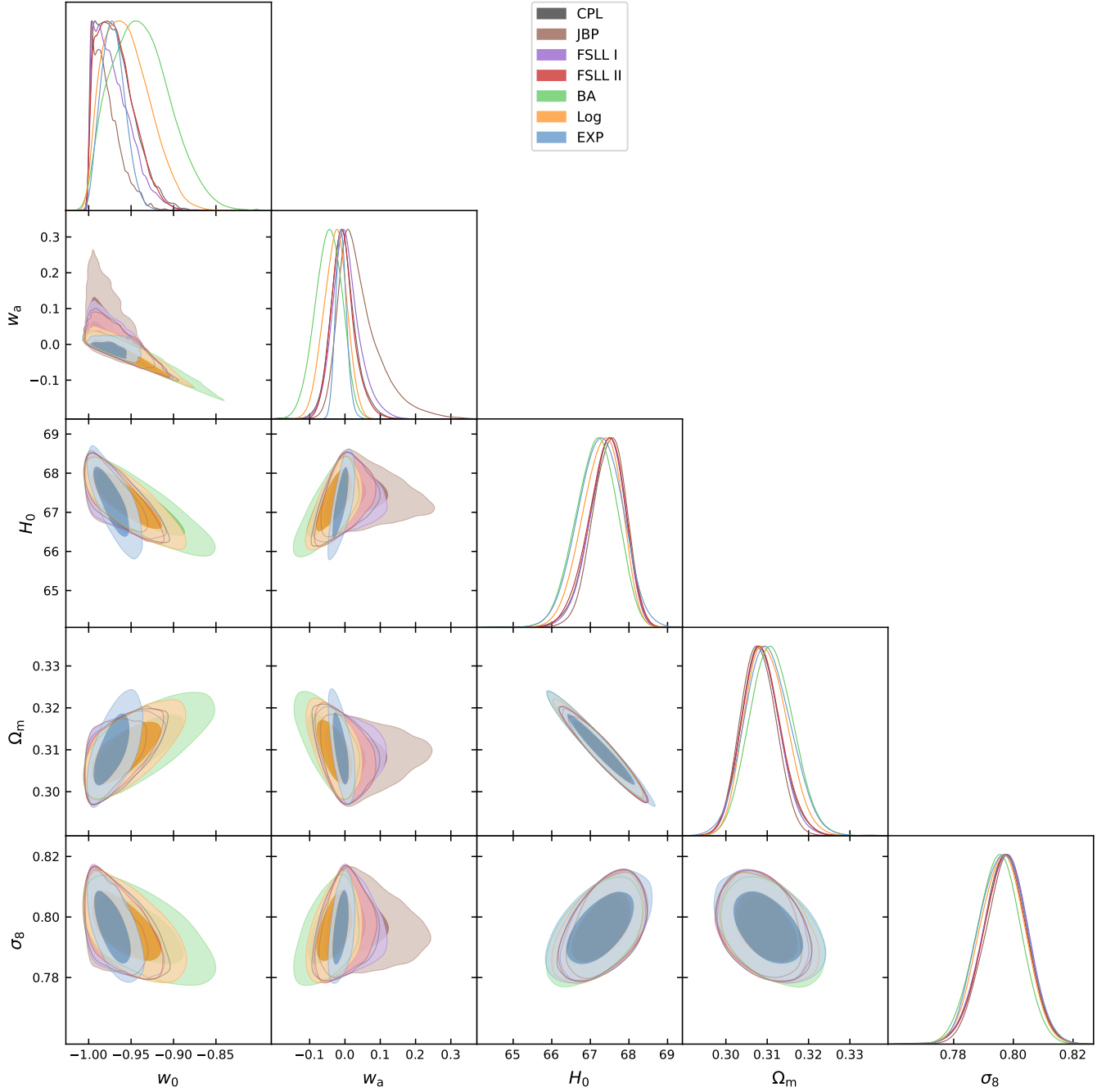


FIG. 10: Comparison of constraints obtained for the models using combined CMB + BAO + PantheonPlus observational datasets.

- [14] D. Scolnic, D. Brout, A. Carr, A. G. Riess, T. M. Davis, A. Dwomoh, D. O. Jones, N. Ali, P. Charvu and R. Chen, *et al.* *Astrophys. J.* **938** (2022) no.2, 113 doi:10.3847/1538-4357/ac8b7a [arXiv:2112.03863 [astro-ph.CO]].
- [15] D. Brout, D. Scolnic, B. Popovic, A. G. Riess, J. Zuntz, R. Kessler, A. Carr, T. M. Davis, S. Hinton and D. Jones, *et al.* *Astrophys. J.* **938** (2022) no.2, 110 doi:10.3847/1538-4357/ac8e04 [arXiv:2202.04077 [astro-ph.CO]].
- [16] D. Rubin, G. Aldering, M. Betoule, A. Fruchter, X. Huang, A. G. Kim, C. Lidman, E. Linder, S. Perlmutter and P. Ruiz-Lapuente, *et al.* [arXiv:2311.12098 [astro-ph.CO]].
- [17] T. M. C. Abbott *et al.* [DES], *Astrophys. J. Lett.* **973** (2024) no.1, L14 doi:10.3847/2041-8213/ad6f9f [arXiv:2401.02929 [astro-ph.CO]].
- [18] B. O. Sánchez *et al.* [DES], *Astrophys. J.* **975** (2024) no.1, 5 doi:10.3847/1538-4357/ad739a [arXiv:2406.05046 [astro-ph.CO]].

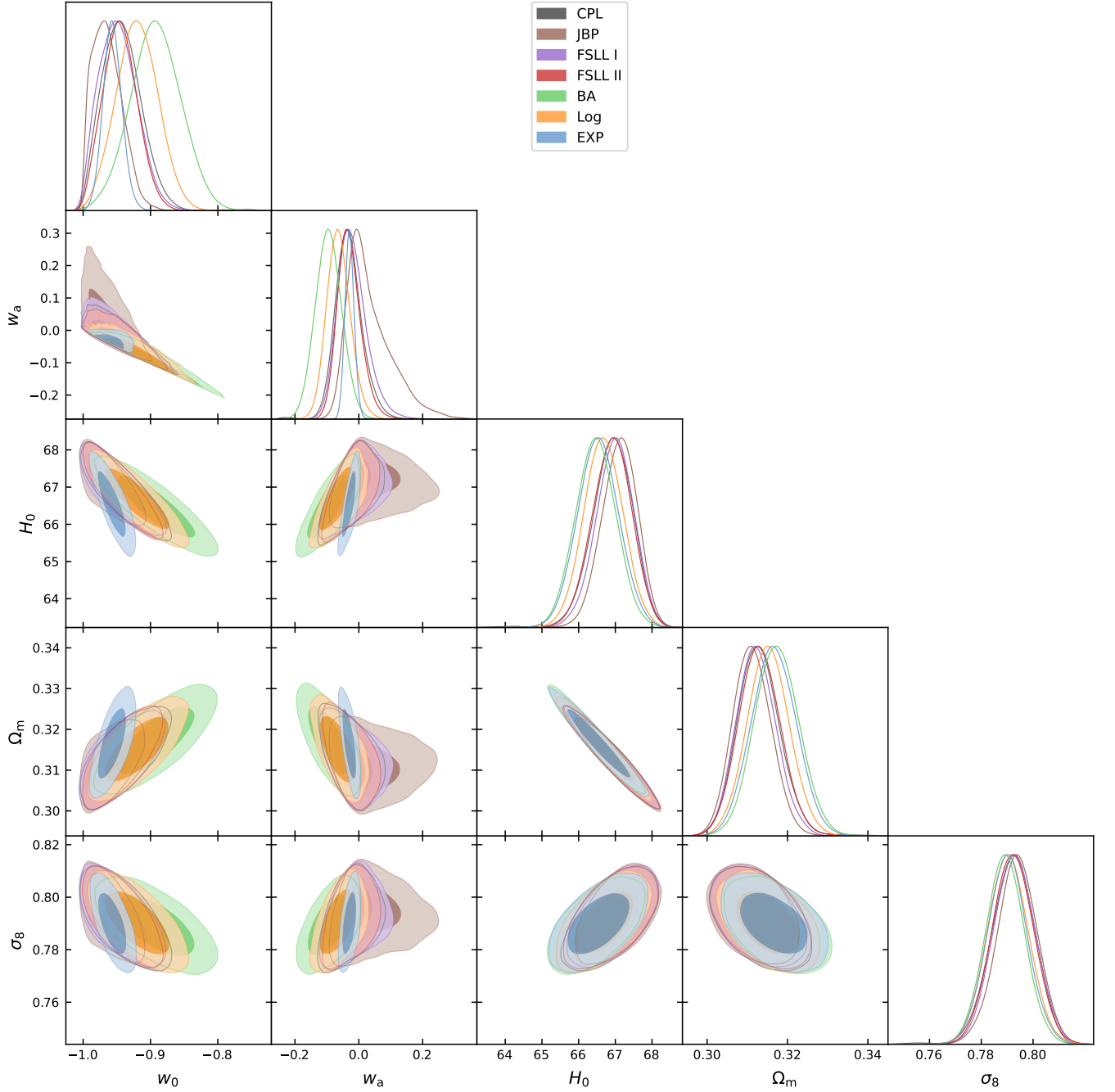


FIG. 11: Comparison of constraints obtained for the models using combined CMB + BAO + DES-Y5 observational datasets.

- [19] M. Vincenzi *et al.* [DES], *Astrophys. J.* **975** (2024) no.1, 86 doi:10.3847/1538-4357/ad5e6c [arXiv:2401.02945 [astro-ph.CO]].
- [20] Z. Wang, S. Lin, Z. Ding and B. Hu, *Mon. Not. Roy. Astron. Soc.* **534** (2024) no.4, 3869-3875 doi:10.1093/mnras/stae2309 [arXiv:2405.02168 [astro-ph.CO]].
- [21] G. Liu, Y. Wang and W. Zhao, [arXiv:2407.04385 [astro-ph.CO]].
- [22] B. Ghosh and C. Bengaly, *Phys. Dark Univ.* **46** (2024), 101699 doi:10.1016/j.dark.2024.101699 [arXiv:2408.04432 [astro-ph.CO]].
- [23] K. Lodha *et al.* [DESI], [arXiv:2503.14743 [astro-ph.CO]].
- [24] U. Andrade *et al.* [DESI], [arXiv:2503.14742 [astro-ph.CO]].
- [25] A. Lewis, A. Challinor and A. Lasenby, *Astrophys. J.* **538** (2000), 473-476 doi:10.1086/309179 [arXiv:astro-ph/9911177 [astro-ph]].
- [26] C. Howlett, A. Lewis, A. Hall and A. Challinor, *JCAP* **04** (2012), 027 doi:10.1088/1475-7516/2012/04/027 [arXiv:1201.3654

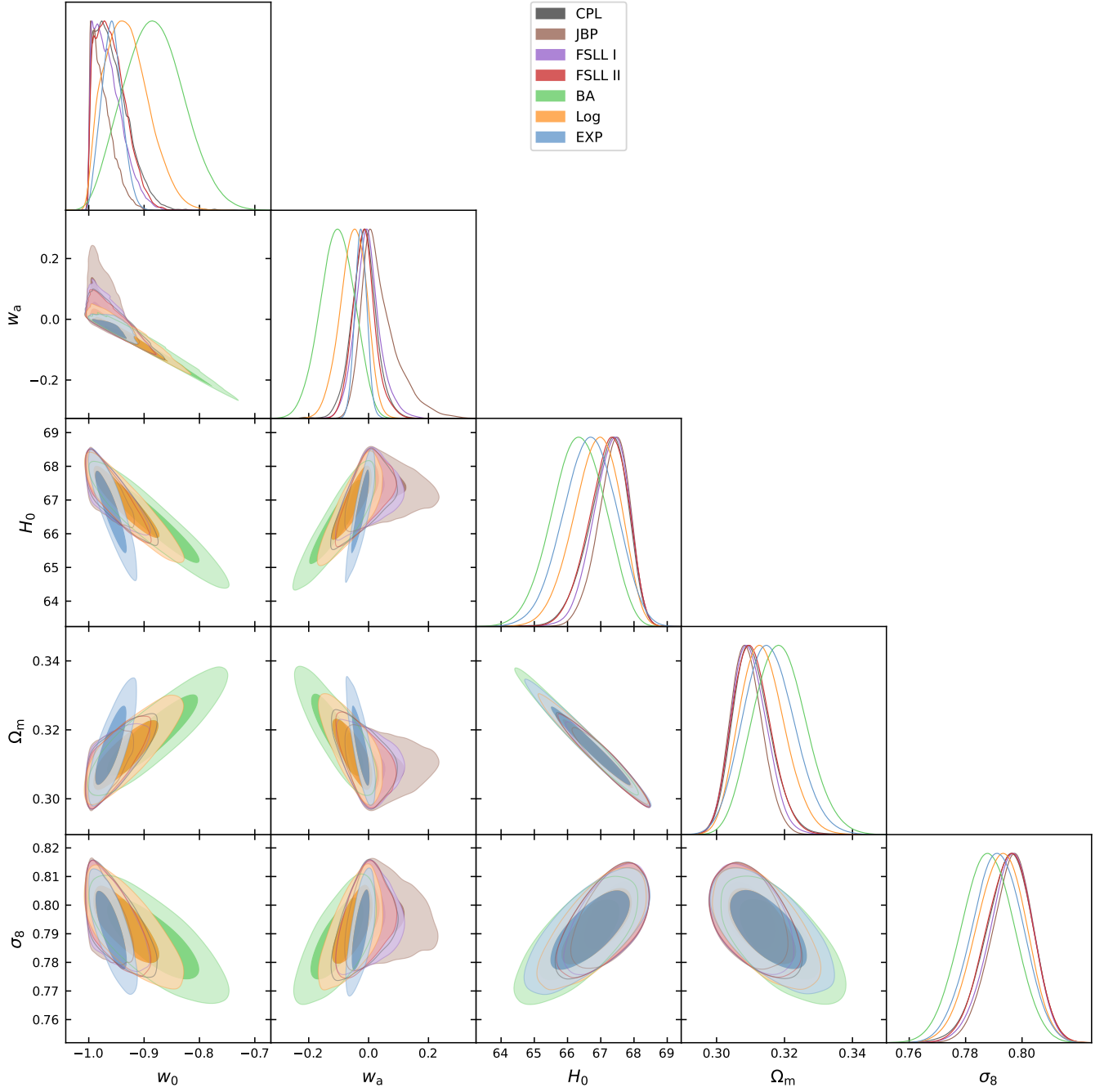


FIG. 12: Comparison of constraints obtained for the models using combined CMB + BAO + Union3 observational datasets.

- [astro-ph.CO]].
- [27] A. Lewis and S. Bridle, Phys. Rev. D **66** (2002), 103511 doi:10.1103/PhysRevD.66.103511 [arXiv:astro-ph/0205436 [astro-ph]].
- [28] A. Lewis, Phys. Rev. D **87** (2013) no.10, 103529 doi:10.1103/PhysRevD.87.103529 [arXiv:1304.4473 [astro-ph.CO]].
- [29] A. Gelman and D. B. Rubin, Statist. Sci. **7** (1992), 457-472 doi:10.1214/ss/1177011136
- [30] E. Rosenberg, S. Gratton and G. Efstathiou, Mon. Not. Roy. Astron. Soc. **517** (2022) no.3, 4620-4636 doi:10.1093/mnras/stac2744 [arXiv:2205.10869 [astro-ph.CO]].
- [31] G. Efstathiou and S. Gratton, doi:10.21105/astro.1910.00483 [arXiv:1910.00483 [astro-ph.CO]].
- [32] J. Carron, M. Mirmelstein and A. Lewis, JCAP **09** (2022), 039 doi:10.1088/1475-7516/2022/09/039 [arXiv:2206.07773 [astro-ph.CO]].
- [33] M. Abdul Karim *et al.* [DESI], doi:10.1103/2wwn-xjm5 [arXiv:2503.14739 [astro-ph.CO]].

- [34] M. S. Madhavacheril *et al.* [ACT], *Astrophys. J.* **962** (2024) no.2, 113 doi:10.3847/1538-4357/acff5f [arXiv:2304.05203 [astro-ph.CO]].
- [35] A. Amon *et al.* [DES], *Phys. Rev. D* **105** (2022) no.2, 023514 doi:10.1103/PhysRevD.105.023514 [arXiv:2105.13543 [astro-ph.CO]].
- [36] L. F. Secco *et al.* [DES], *Phys. Rev. D* **105** (2022) no.2, 023515 doi:10.1103/PhysRevD.105.023515 [arXiv:2105.13544 [astro-ph.CO]].
- [37] F. Beutler, C. Blake, M. Colless, D. H. Jones, L. Staveley-Smith, L. Campbell, Q. Parker, W. Saunders and F. Watson, *Mon. Not. Roy. Astron. Soc.* **416** (2011), 3017-3032 doi:10.1111/j.1365-2966.2011.19250.x [arXiv:1106.3366 [astro-ph.CO]].
- [38] A. J. Ross, L. Samushia, C. Howlett, W. J. Percival, A. Burden and M. Manera, *Mon. Not. Roy. Astron. Soc.* **449** (2015) no.1, 835-847 doi:10.1093/mnras/stv154 [arXiv:1409.3242 [astro-ph.CO]].
- [39] S. Alam *et al.* [BOSS], *Mon. Not. Roy. Astron. Soc.* **470** (2017) no.3, 2617-2652 doi:10.1093/mnras/stx721 [arXiv:1607.03155 [astro-ph.CO]].
- [40] P. J. Wu, *Phys. Rev. D* **112** (2025) no.4, 043527 doi:10.1103/mcgb-ntwr [arXiv:2504.09054 [astro-ph.CO]].
- [41] M. Chevallier and D. Polarski, *Int. J. Mod. Phys. D* **10** (2001), 213-224 doi:10.1142/S0218271801000822 [arXiv:gr-qc/0009008 [gr-qc]].
- [42] E. V. Linder, *Phys. Rev. Lett.* **90** (2003), 091301 doi:10.1103/PhysRevLett.90.091301 [arXiv:astro-ph/0208512 [astro-ph]].
- [43] R. Shah, P. Mukherjee and S. Pal, *Mon. Not. Roy. Astron. Soc.* **536** (2024) no.3, 2404-2420 doi:10.1093/mnras/stae2712 [arXiv:2404.06396 [astro-ph.CO]].
- [44] H. K. Jassal, J. S. Bagla and T. Padmanabhan, *Phys. Rev. D* **72** (2005), 103503 doi:10.1103/PhysRevD.72.103503 [arXiv:astro-ph/0506748 [astro-ph]].
- [45] H. Chaudhary, S. Capozziello, V. K. Sharma, I. Gómez-Vargas and G. Mustafa, [arXiv:2508.10514 [astro-ph.CO]].
- [46] W. Giarè, M. Najafi, S. Pan, E. Di Valentino and J. T. Firouzjaee, *JCAP* **10** (2024), 035 doi:10.1088/1475-7516/2024/10/035 [arXiv:2407.16689 [astro-ph.CO]].
- [47] C. J. Feng, X. Y. Shen, P. Li and X. Z. Li, *JCAP* **09** (2012), 023 doi:10.1088/1475-7516/2012/09/023 [arXiv:1206.0063 [astro-ph.CO]].
- [48] D. Staicova, *Universe* **8** (2022) no.12, 631 doi:10.3390/universe8120631 [arXiv:2211.08139 [astro-ph.CO]].
- [49] E. M. Barboza, Jr. and J. S. Alcaniz, *Phys. Lett. B* **666** (2008), 415-419 doi:10.1016/j.physletb.2008.08.012 [arXiv:0805.1713 [astro-ph]].
- [50] D. Kumar, A. Mitra, S. A. Adil and A. A. Sen, *Phys. Rev. D* **111** (2025) no.4, 043503 doi:10.1103/PhysRevD.111.043503 [arXiv:2406.06757 [astro-ph.CO]].
- [51] G. Efstathiou, *Mon. Not. Roy. Astron. Soc.* **310** (1999), 842-850 doi:10.1046/j.1365-8711.1999.02997.x [arXiv:astro-ph/9904356 [astro-ph]].
- [52] S. Arora, A. De Felice and S. Mukohyama, [arXiv:2508.03784 [gr-qc]].
- [53] N. Aghanim *et al.* [Planck], *Astron. Astrophys.* **641** (2020), A5 doi:10.1051/0004-6361/201936386 [arXiv:1907.12875 [astro-ph.CO]].
- [54] N. Dimakis, A. Karagiorgos, A. Zampeli, A. Paliathanasis, T. Christodoulakis and P. A. Terzis, *Phys. Rev. D* **93** (2016) no.12, 123518 doi:10.1103/PhysRevD.93.123518 [arXiv:1604.05168 [gr-qc]].
- [55] S. Pan, W. Yang and A. Paliathanasis, *Eur. Phys. J. C* **80** (2020) no.3, 274 doi:10.1140/epjc/s10052-020-7832-y [arXiv:1902.07108 [astro-ph.CO]].